

INITIAL DEVELOPMENT OF THE CUBESAIL/ULTRASAIL SPACECRAFT

R. L. Burton, J. K. Laystrom-Woodard, G. F. Benavides, and D. L. Carroll
CU Aerospace, L.L.C.
Champaign, IL

V. L. Coverstone, G. R. Swenson, A. Pukniel, A. Ghosh, and A. D. Moctezuma
University of Illinois at Urbana-Champaign
Urbana, IL

ABSTRACT

The UltraSail spacecraft can potentially achieve square-kilometer sail areas by deploying sail blades between satellites separated by as much as 5000 m. In the UltraSail version, the spacecraft spins about a central hub to flatten the blades against photon pressure, supported by tip-satellites. The sail is launched in a rolled-up “window-shade” configuration, allowing sail storage and deployment to very large areas without folding. Spacecraft control of the thrust vector by spin-axis slewing is achieved by twisting the blades with the tip-satellites. Propellant mass fraction is very small, allowing use of cold gas even for high- ΔV interplanetary missions. CubeSail is designed as a low-cost demonstration of UltraSail, using two near-identical CubeSat satellites to deploy a 250 m-long, 20 m² reflecting film between them. A minimum altitude of 750 km is needed to minimize aerodynamic forces. The two satellites are launched as a unit, detumbled, and separated, with the film unwinding symmetrically from motorized reels in the payload bays. It is found that gravity-gradient is preferred over spinning as a way to provide the necessary tension in the film. CubeSail design and experimental development is described.

INTRODUCTION

Many solar sail designs [Vulpeti, 2008] employ masts and rigging for sail deployment. Mast systems limit sail performance in two ways, in that the mass of the mast reduces spacecraft acceleration, and the mast length is limited structurally, therefore limiting the sail area.

Attempts to overcome mast limitations go back to the Heliogyro [MacNeal, 1967][MacNeal, 1971] (Fig. 1), which employed radial blades attached to a central core, centrifugally spun to provide stiffness. While the Heliogyro could in principal achieve very large areas (MacNeal envisioned blade lengths up to 30 km), blade control issues existed. Achieving the initial spin-up would be difficult, and the damping of radial waves is difficult at the free end. Blade response is relatively slow, requiring approximately 2/3 of a revolution (~2 radians) for a commanded pitch wave to travel from the core to a blade tip and back.

UltraSail (Fig. 2), which builds on Heliogyro heritage by using a spinning blade system attached to a central hub, was conceived to improve control by adding a low-mass controllable satellite (tipsat) at the tip of each blade [Botter, 2008][Hargens-Rysanek, 2007]. By initiating blade control at the tip, instead of at the hub, blade response is improved to approximately 1/3 of a revolution (~1 radian) for a commanded pitch wave to travel from to a blade tip to the hub. This added control reduces the spin rate, enables blade pitch control for spin-up.

Approved for public release; distribution is unlimited.

This effort was performed under contract NNX09CB37C with NASA Marshall Space Flight Center.

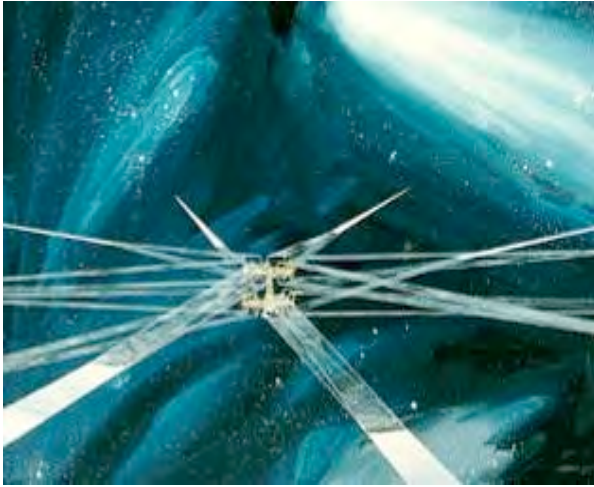


Figure 1: Heliogyro.

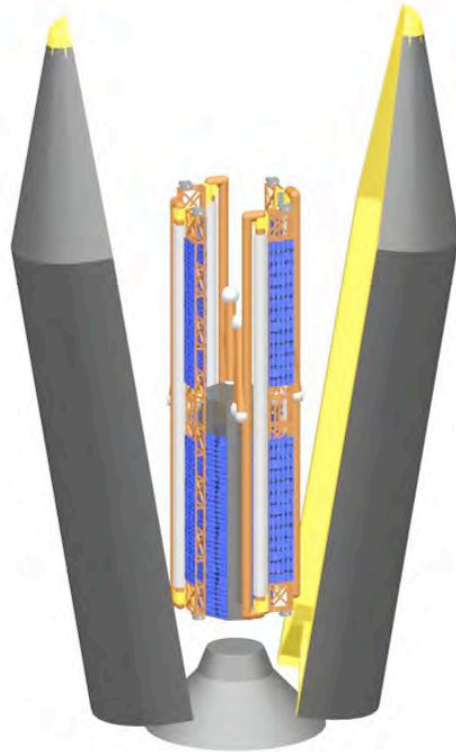


Figure 2: UltraSail launch configuration.

ANALYSIS IN TERMS OF THE ROCKET EQUATION

The spacecraft designer can consider an electric propulsion system on a high ΔV spacecraft in terms of three subsystems:

$$\text{total mass} = \text{transfer mass (bus + payload + power source)} + \text{propellant}$$

For a solar sail vehicle:

$$\text{total mass} = \text{transfer mass (bus + payload)} + \text{solar sail}$$

The solar sail thus plays the same role as propellant on a conventional spacecraft. A major advantage of the “propellantless” solar sail is that the need for a relatively massive and expensive power source is avoided.

The equivalent specific impulse and power of a solar sail are found from the rocket equation, written as:

$$\text{characteristic velocity } (\Delta V) = (g \cdot \text{specific impulse}) \ln[(\text{total mass})/(\text{total mass} - \text{solar sail mass})]$$

so that the effective “exhaust velocity” $U_e = gl_{sp}$ is:

$$U_e = gl_{sp} = \Delta V / \ln\left(\frac{m_o}{m_o - m_{ss}}\right)$$

By analogy with electric systems, in terms of thrust T the solar sail power is $P_{ss} = \frac{1}{2} T U_e$. Writing thrust in terms of the solar pressure P_o as

$$T = 2P_o A_{ss} = 2P_o m_{ss} / \sigma$$

where σ is the areal specific mass in kg/m^2 . For $m_{ss}/m_0 = \mu_{ss}$, the power is:

$$P_{ss} = \frac{1}{2} T U_e = P_o m_{ss} \left(\frac{\Delta V}{\sigma \ln \frac{1}{1-\mu_{ss}}} \right)$$

For systems with $\mu_{ss} \ll 1$:

$$P_{ss} \cong \frac{P_o m_{ss} \Delta V}{\sigma \mu_{ss}}$$

To compare solar sail systems with electric systems, it is convenient to compare the specific mass α [kg/W]:

$$\alpha = \frac{m_{ss}}{P_{ss}} = \frac{\sigma \mu_{ss}}{P_o \Delta V}$$

As an example, consider a sail with an areal density of $5 \text{ [g/m}^2\text{]}$, $\mu_{ss} = 0.1$, $P = 4 \times 10^{-6} \text{ [N/m}^2\text{]}$, and $\Delta V = 25 \text{ km/s}$, giving $\alpha = 5 \text{ g/W} = 5 \text{ kg/kW}$.

An α of 5 kg/kW is very competitive when compared to electric systems, for which α is typically 20 kg/kW [Bonfiglio, 2005]. For example, a mass comparison of ($a \Delta V$) = 20 km/s solar electric and solar sail mission, where the power level is 30 kW , is given in Table 1.

Table 1: Mass comparison of solar electric vs. solar sail missions.

	NEXT Solar Electric (SEP)	Solar Sail (SS)
Mission ΔV [km/s]	20	20
Bus + payload mass [kg]	1600	1600
Launch mass [kg]	3300	1800
Acceleration [mm/s^2]	0.21	0.21
Thrust at 1 AU [N]	0.70	0.35
Propellant + tank [kg]	1300	0
Propulsion mass [kg]	400	200
Eff. Specific impulse [s]	4000	20,000
Effective power [kW]	20	35
Sail area [m^2]	--	40,000
Launch Vehicle	Delta IV Medium	Falcon 9
Launch Cost	\$160 M	\$50 M
Propulsion Cost	(est.) \$100 M	TBD

ULTRASAIL CONCEPT

UltraSail was conceived as a way to achieve extremely high solar sail performance by minimizing sail support hardware coupled with 1 km^2 -class sail areas [Burton, 2005]. Sail material is mounted on multiple reels, each with a width of $5 - 10 \text{ m}$, and deployed to a blade length up to 5000 m . Deployment

and blade control is enabled with a satellite (tipsat) attached to each blade tip (Figs. 3 – 4). Calculated performance exceeds that of solar electric propulsion systems.

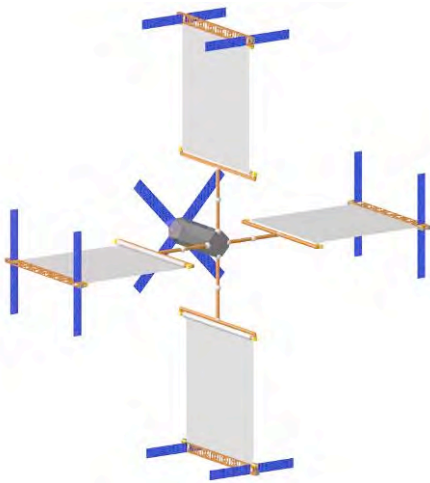


Figure 3: UltraSail deployment.

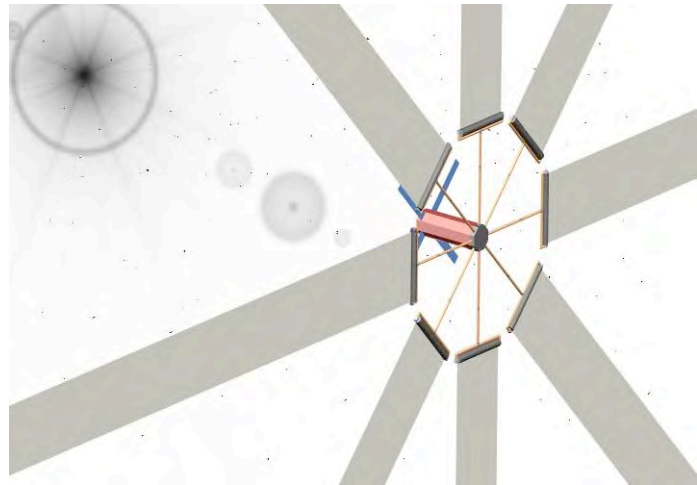


Figure 4: UltraSail blades deploy from a central hub to achieve a km²-class sail area.

The baseline design for UltraSail assumes the use of a coated polyimide film with ripstop. UltraSail blade stiffness is achieved by spinning the spacecraft. Total film stress due to rotation is a few per cent of yield, not including the strength added by the ripstop.

Fully deployed, each tipsat performs a circular orbit about the central hub, with rotational axis generally pointing at the sun. The tip-satellite, a lightweight beam truss with onboard propulsion, performs the following functions:

1. A stable, stiff attachment point for the film end.
2. Bus for propellant, solar panels, thrusters, and a metrology system.
3. On-board thrust to initiate film roll-out and initial blade spin.
4. Satellite metrology system to provide blade tip position, velocity and acceleration.
5. Twists (pitches) the blades to induce torques for spin-stabilization, using pitch thrusters.
6. Satellite centrifugal force flattens blade to increase photon thrust.
7. Provides continuous plane-change control for Sun-orientation of spacecraft spin axis.
8. Blade camber control to stabilize orientation along the blade axis.

Therefore, if the tip-satellite is very small, the possibility exists for extremely low areal densities approaching the areal density of the film itself.

The rotation of the film and blade mass provide centrifugal force that tends to prevent the blade from blowing back due to the solar pressure P_0 . Dynamic models have shown that the optimum spin rate achieves a total centrifugal force on a blade of 3 – 5 times the solar pressure force. For km-long blades this results in a rotational period of 1 – 2 hours, and a tip speed of 10s of m/s.

SOLAR RADIATION PRESSURE

A right-handed orthogonal coordinate system was constructed by defining the z-axis to coincide with the spin axis of the UltraSail. Positive z was defined to be in the direction away from the sun. The x-axis was defined to be normal to the z-axis in the direction of an undeflected blade. Note that this coordinate system rotates with the blade. Because the rotating blades are not rigidly attached to the hub, they will be deflected away from the Sun due to the photon force until equilibrium is achieved between centrifugal

force and photon force. In this analysis, the blades were assumed to remain straight, even though in reality they will assume a catenary shape of the form:

$$z(x) = -\frac{P_o}{\omega^2} \left[\frac{cx_m \operatorname{arctanh} \left[x \left(\frac{\rho c}{2m_{\text{sat}}R + \rho cR^2} \right)^{1/2} \right]}{\left[\rho cR/2(m_{\text{sat}} + \rho cR/2) \right]^{1/2}} + \frac{\ln \left[\omega^2 (m_{\text{sat}}R + \rho cR^2/2 - \rho cx^2/2) \right]}{\rho} \right]$$

where $x_m = R[1 - m_{\text{sat}}/(M/N + m_{\text{sat}})]$. The above equation gives deflection in the z direction as a function of the x coordinate of the point along the centerline of the sail. For small deflection angles, the pressure on a catenary blade shape versus a straight blade will be nearly identical. The necessity to display maximum possible solar sail area to the Sun precludes large deflection angles, and thus the straight blade assumption is valid (Fig. 5).

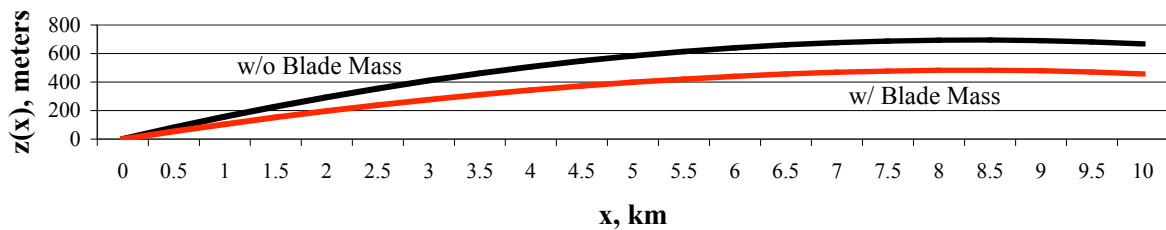


Figure 5: Catenary Shape. The tipsat deflection angle (w/ blade mass) is 2.6 deg.

In the UltraSail design, the amount of this deflection can be controlled by the angular velocity of the blades (at higher angular velocities, the deflection angle, ζ , will decrease due to higher centrifugal force). As will be discussed later, part of this work involved finding the amount of centrifugal force that yielded the optimal deflection angle, based on increased or decreased fuel consumption of the tip-satellites and the associated changes in tip-satellite mass.

Subsystem mass analysis for the tip-sat and hub was conducted to provide baseline masses for the calculations performed above. Subsystems studied for the tip-satellites include propulsion, avionics, power, structure, and the blade deployment mechanism/compliant attachment.

The main structure of the tip-satellites consists of a simple truss, constructed of either aluminum or carbon fiber tubes. The structure is 5 m long with a $0.5 \times 0.5 \text{ m}^2$ cross section. The truss structure consists of 10 half meter cube elements, with cross members on each face of the cube, Fig. 6. Using half inch carbon fiber tube with a 0.8 mm wall thickness for the truss, yields a mass of 4.6 kg. Fittings, attachment points, and passive thermal control systems bring the total structure mass up to 8.0 kg.

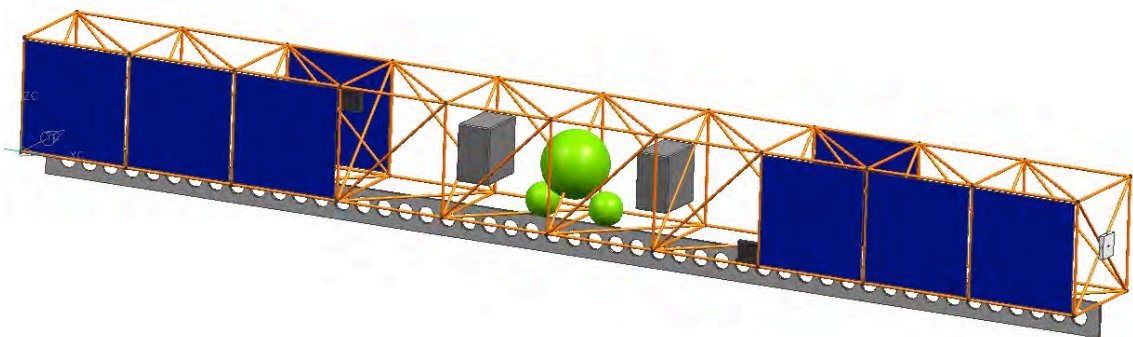


Figure 6: Tipsat. 27 kg tipsat supports 71 kg of film.

The avionics system is relatively complex because of the need for relatively decent positioning data. Therefore, each tip-satellite has two Sun-sensors and two star-trackers, for redundancy. Further, the positioning information is gathered with a microwave ranging system as described in the ranging section. Computation is done at the hub in near-real time to achieve nearly autonomous operation; a modest communications system is necessary to relay the information between hub and tip-satellite. These communications are also necessary for the relay of other pertinent subsystem data, commands, and state of health.

The power subsystem consists of body-mounted solar panels and associated power processing equipment. Beginning-of-life estimates for solar panel specific power are 50 W/kg. Power requirements for the tip-sat are assumed to be 50 W, yielding 1 kg in solar arrays per satellite. Additional processing equipment and batteries are another 2 kg.

The propulsion system on the tip-sat consists of 2 thruster units mounted on either end of the truss structure, providing thrust on the order of 0.1 N. These units utilize catalyzed nitrous oxide (N_2O), to yield approximately 150 s I_{sp} . The attitude control system consists of nearly identical thrusters, also mounted on the ends of the truss and providing thrust on the order of 10 mN, using cold butane. Depending on film thickness, mission lengths and force ratios, the propellant mass varies between 1 and 20 kg. Assuming a pressure fed system, with a chamber pressure of 750 psi and Titanium tanks tank mass was determined as a function of initial propellant mass, and ranged from 1 – 6 kg.

It was shown that a tip-satellite dry mass of approximately 42 kg and a hub dry mass of just under 50 kg is possible with state of the art technology. This is encouraging from the standpoint of minimizing areal density of the combined blade and tip-sat system.

The final part of this analysis was to determine the most appropriate force ratio for a given mission length. The force due to solar pressure for the baseline UltraSail design when the deflection angle ζ is zero is 0.228 N, the maximum possible force. For large deflection angles, (low force ratio) the blade length needs to be increased as the force drops with the cosine of the deflection angle. For each new blade length, and hence increased blade mass, the angular velocity of the system was assumed to remain the same. Because blade length increased and angular velocity remained the same, the tip velocity increases. This change requires a new value for the amount of propellant and tank mass. A new, greater, tip-sat mass was then calculated and the problem repeated until it converged. These increases were summed for all four satellites and blades.

The total mass of the four tip satellites and blades are plotted as a function of force ratio for varying mission lengths in Fig. 7, which shows a force ratio for minimum tip-satellite and blade mass. This optimum force ratio runs between 3 and 3.5 for the higher mission lengths. For the two year mission, the minimum is at a force ratio around 5. However, the payload mass gain is so minimal between 3.5 and 5 that it does not seem necessary to operate the UltraSail at higher force ratios. For the baseline UltraSail design, a force ratio of 3 was adopted.

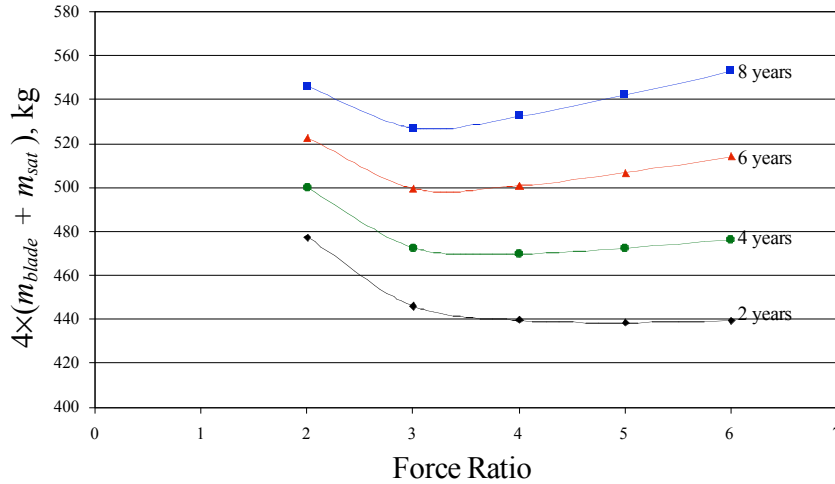


Figure 7: Mass of all Tip-Satellites and Blades vs. Force Ratio for 4 Mission Durations.

VACUUM DEPLOYMENT EXPERIMENT

One of the most challenging aspects of the UltraSail project is the deployment of a potentially kilometers-long sail from a rolled up configuration. The Vacuum Deployment Experiment (VDE) measures the required force to unwind the sail material from the reel in a vacuum environment as a function of speed. Also, the experiment is designed to be portable enough to allow it to be placed on board a micro-gravity simulation aircraft, to study unrolling in a zero-g environment.

Two reels are placed in a vacuum chamber (Fig. 8). One reel is pre-wrapped with 100 meters of 30 cm wide, 2.5 micron film from SRS technologies, and the other reel acts as a take up. The reels are synchronized by a timing belt, and connected to a precision variable speed motor on the outside of the tank by a ferro-fluidic rotary motion vacuum feedthrough. The force transducer shown in Fig. 8 indirectly measures the tension in the sail material at different unwinding speeds, to a maximum force of 125 g. By closely measuring the angles of the film between the reels and the roller, along with the measured force, the film tension can be calculated, which is equivalent to the peel force. The unwinding force overcomes the peeling force, which is the sum of the electrostatic and adhesive forces between the sail surfaces. The tension measurement system is shown in Fig. 8; Fig. 9 shows the vacuum chamber.

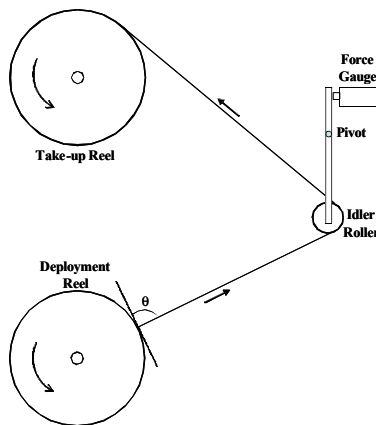


Figure 8: Tension measurement system.

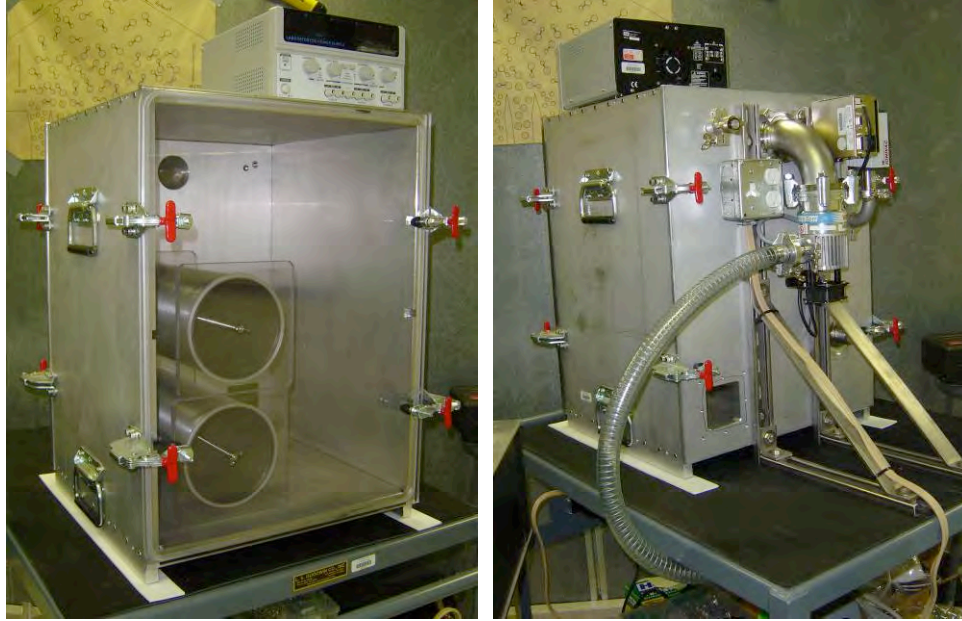


Figure 9: Vacuum Deployment Experiment (front and back).

The peeling force is in general an unknown function of unwinding speed. The required unwinding force will be provided by tip satellites and/or by centrifugal force. The expected tension range is very small (0 - 10 mN), so the experiment was designed to measure these small forces. Unwinding speeds up to 1 m/s were simulated by the experiment.

Initial experiments were performed with a filled teflon slit material. It was found that the peel force increased with time, and soon became excessive, due to electrostatic forces. Efforts to drain off electrostatic charge with a grounding brush failed, and the slit was then fabricated with aluminum.

The aluminum slit was highly successful. The peel force was too small to measure, and no electrostatic charge buildup was observed. It was concluded that the film could be deployed even with the small forces available in orbit due to gravity gradient or spacecraft spin.

CUBESAIL CONCEPT

It was concluded that a low cost way to test the UltraSail concept would be to use two CubeSats, nearly identical, with the film deployed between them (Fig. 10). The spacecraft is called CubeSail. Each CubeSat holds approximately 8 cm x 125 m (10 m²) of 6.2 mm double-coated Mylar film. The spacecraft mass is ~2.5 kg, and the film mass is ~90 g. The total mass of the film, deployment equipment, and associated electronics is ~500 g.

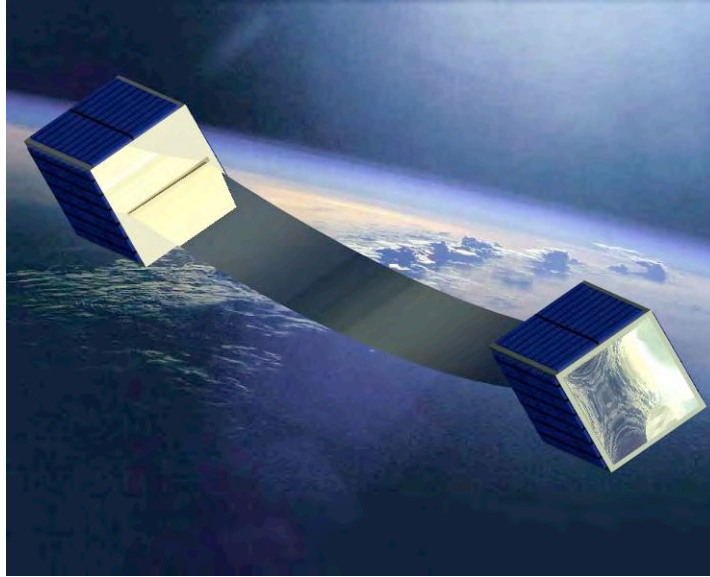


Figure 10: Artist's rendition of CubeSail solar sail deployment.

The relatively slow emergence of solar sailing as a viable space propulsion method can be traced to three challenges: low technology readiness level, complications related to stowage, deployment, and support of large flexible structures, and control of the large flexible spacecraft. To address these challenges, we proposed a small-scale (20 m^2) demonstration of deployment, sail performance during nominal operations, and orbital maneuvering in low Earth orbit (LEO). The low Earth orbit environment poses unique challenges for a 20 m^2 solar sailing spacecraft, including time-varying lighting conditions, residual atmospheric drag disturbance torques, and potential of film damage due to micro-meteorite debris. Despite these challenges, deployment into a low Earth orbit is chosen in order to take advantage of highly reduced launch costs as secondary payload, and to advance the technology readiness level (TRL) of several CubeSail subsystems. The spacecraft fully conforms to the CubeSat Design Specifications [Cal Poly SLO, 2009] and can thus be integrated with the space-qualified Poly-Pico Satellite Deployer (P-POD), shown in Fig. 11. This ability not only reduces complexity in integrating our spacecraft with the launch vehicle, but also instills confidence in the safety of the primary payload and facilitates unproblematic deployment into a desired orbit.



Figure 11: Poly-Pico Satellite Deployer [Cal Poly SLO, 2010].

The CubeSail mission is a first in a series of increasingly complex demonstrations leading up to a full-scale UltraSail mission. The primary mission objective is to test the reel-based stowage and deployment mechanism that eliminates traditional sail support structures such as booms, masts, stays, or guy-wires.

The film is wound onto two motor-driven, variable-speed reels, each placed in a 15x10x10 cm tip satellite. Internal to the reel is the motor, magnetic encoder for measuring deployment rate and length, and related wiring. The sail material is a polyimide-based polymer coated on the front side with aluminum to achieve maximum reflectivity and to ensure that equilibrium temperature is within the operating range of the base polymer. In addition, the film is reinforced with ripstop thread to prevent tear propagation in the event of film damage. The resulting total film thickness is 6.2 μm . The payload bay constraint on film width of 78 mm results in total film length of 260 m, split evenly between the two CubeSats.

The top-level mission sequence of the CubeSail begins with P-POD ejection and separation of the spacecraft from the upper stage of the launch vehicle, followed by bus power-up and internal health checkout procedures. The batteries are allowed to recharge and initial ground communication is established using an omnidirectional antenna. After successful checkout and verification of nominal operations of all subsystems, the satellite initiates despin and reorientation. During this phase, the two CubeSats are held rigidly together using the SRU and are oriented with its long axis along the nadir direction with zero rotational velocity. Attitude determination and control methods, including sensor suite and actuators, are discussed in greater detail in a subsequent section.

Once CubeSail is despun and oriented along the nadir, the batteries are allowed to fully recharge and the separation sequence is initiated. First, film tension is released. The SRU motor is then started and is rotated four turns until the satellites are separated. Guide pins ensure both spacecraft are locked in the pitch direction and that the separation occurs linearly. The film is now in tension from two separation springs, which provide initial separation velocity.

After the SRU operation is complete, film deployment is initiated by engaging the reel motor and running it at a prescribed time-varying rate until full 260 m of sail are deployed. The gravity gradient force ensures that sufficient tension exists in the film to prevent excessive billowing due to solar radiation pressure and residual aerodynamic drag. Details regarding the deployment dynamics are presented in a subsequent section.

The desired insertion orbit is selected based on several design criteria, the most important of which is a constant lighting condition. Avoiding transitions between sunlit and dark portions of the orbit minimizes time-varying dynamic loading of the sail. In orbits which do not guarantee constant lighting conditions, the sail billowing will increase during the sunlit portions and decrease during the dark portion, creating an accordion-like effect on the CubeSats. The non-constant force ratio between solar radiation pressure and gravity gradient can cause damage to the film and must be minimized. Additionally, orbits with constant lighting avoid thermal cycling of the sail material, and offer much easier planning of orbital maneuvers. As a result, CubeSail's target orbit is the sun-synchronous terminator orbit, shown in Fig. 12.

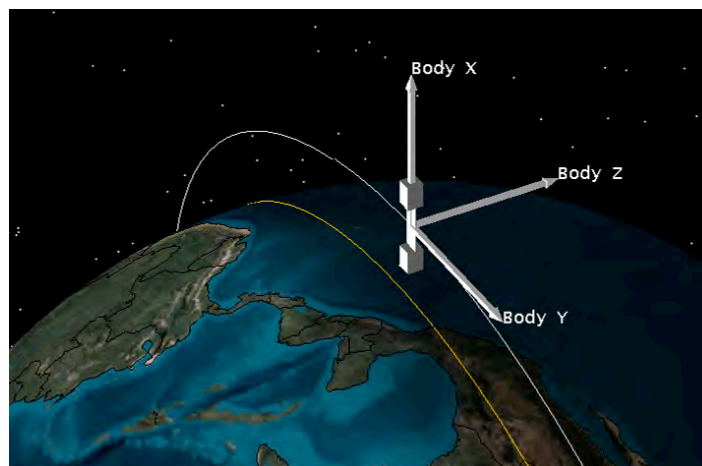


Figure 12: CubeSail in sun-synchronous terminator orbit. Image is not to scale and shows no billowing effects. The yellow line on the surface indicates the solar terminator.

The desired insertion altitude into the sun-synchronous orbit is selected to achieve a baseline one year orbital lifetime. The plot and associated table, Fig. 13 and Table 2, show the relationship between insertion altitudes and orbital lifetime for various attitudes and times within the solar cycle. The variations in solar flux over the 11 year sun cycle cause fluctuations in the Earth's atmospheric density by as much as two orders of magnitude and therefore must be carefully taken into account. The calculations were performed using the Naval Research Laboratory's NRLMSISE2000 atmospheric density model [Naval Research Laboratory, 2000] and the Analytical Graphics Incorporated Satellite Tool Kit Lifetime analysis tool. The shaded areas in the table represent altitudes at which the spacecraft will survive at least 1 year before deorbiting, for each of the described attitudes. It is important to note that for the worst case scenario when the sail is face-on to the velocity vector, the spacecraft must be deployed into a 800 km orbit during solar minimum and 900 km orbit during solar maximum.

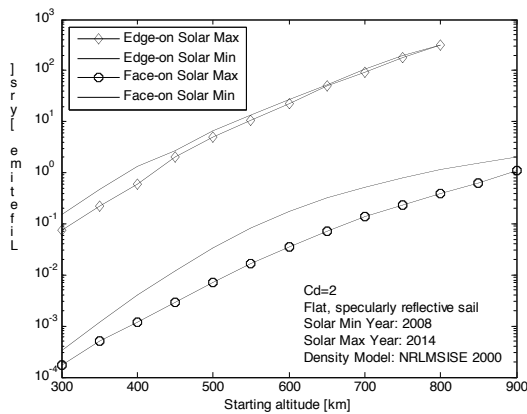


Figure 13: Orbital lifetime predictions for various attitudes, solar cycle intervals, and altitudes.

Table 2: Orbital lifetime with respect to insertion altitude and solar cycle.

Alt (km)	Orbital Lifetime (yrs)			
	Edge-on Sol Min	Edge-on Sol Max	Face-on Sol Min	Face-on Sol Max
400	1.4	0.6	0.004	0.0012
500	6.7	4.9	0.034	0.0073
600	27.2	22.4	0.176	0.0036
700	106	92.5	0.508	0.137
800	317	316	1.169	0.386
900	>300	>300	2.044	1.108

Although the launch date within the solar cycle has a significant effect on the orbital lifetime, the sail attitude with respect to the velocity direction has an even greater impact. From the above table, during a solar maximum period, if the film is deployed with the sail normal perpendicular to the velocity direction (edge-on) and must survive for at least one year, it must be deployed into a minimum initial altitude of 500 km. In contrast, if the sail is deployed in the face-on configuration during the same period, it must be inserted into a 900 km initial orbit. As a result of this strong dependence of orbital lifetime on CubeSail attitude, the spacecraft is nominally flown in the zero pitch (edge-on) configuration. During orbital maneuvers, the CubeSats can be pitched in opposite directions, inducing a twist in the film and creating a net force. Appropriate pitching maneuvers are thus used to produce changes in orbital inclination and altitude and demonstrate CubeSail's solar radiation pressure maneuvering capability.

BUS AND GROUND COMMUNICATIONS

CubeSat is based on the IlliniSat-2 bus, designed to be a fully modular, highly adaptable system that is fully compatible with the CubeSat and P-POD standards. The satellite bus consists of power, command and data handling (C&DH), and attitude determination and control (ADCS) subsystems. The IlliniSat-2 bus in a 1.5U structure has a mass of about 900 grams and the bus electronics fit into less than a 1U cube as shown in Fig. 14. As such, the bus provides excellent mass margin (~1100 grams) and volume margin (~9x9x8 cm) for payloads/instruments. The system is constructed as a set of sub-assemblies, allowing pre-integration testing of the payload and service modules independently. The IlliniSat-2 bus builds on experience gained in the design of ION1 and makes extensive use of emerging technologies that will serve to push the envelope of future CubeSat missions. Extensive ground testing of the bus outlined in the supplementary document will ensure mission success, despite the lack of flight heritage for the current design.

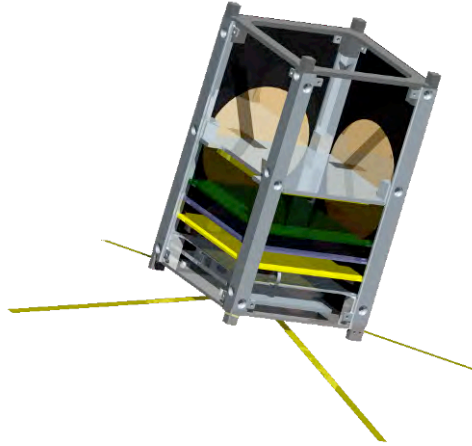


Figure 14: Generic IlliniSat-2 bus in a 1.5-U configuration.

POWER SUBSYSTEM

The power subsystem consists of four body-mounted solar panels, a lithium-ion battery pack, and supporting circuitry required to operate the spacecraft and associated science payload. Each solar panel consists of 3 Spectrolab triple junction solar cells (25% QE) mounted on a light-weight carbon fiber panel. The carbon fiber backing provides a significant mass reduction over typical FR4 fiberglass panels. Maximum operating efficiency of each string of solar cells is maintained via power point tracking. Power collected from the cells is directed through a battery charger to maintain and charge a lithium-ion battery pack (7.4 V, 2200 mAh). Solar panels occupy the four largest of the six faces of the CubeSat. A six-month simulation of a nominal mid-latitude orbit (45° inclination) indicates that 2 W of on-orbit average power will be produced in the 1.5-U configuration, which is sufficient for the proposed CubeSail mission.

The power board has high efficiency (>85%) switching voltage regulators to provide 5 VDC for the satellite bus. Additionally, 8 switched lines from the battery (7.4 VDC) are available for the radio and additional heaters/high current loads as required. Each regulator has been designed for maximum power efficiency and the power subsystem is intelligently controlled and monitored via a microcontroller on the power PCB that coordinates power control with the C&DH motherboard.

C&DH SUBSYSTEM

The C&DH subsystem controls the operation of the spacecraft and provides communication with the ground station. The C&DH motherboard includes a Texas Instruments OMAP5912 processor and system memory, including random access memory (64 MB) for program operation and non-volatile flash memory (> 1 GB) for data and program storage. Included in the C&DH subsystem are PIC microcontrollers that reside on the power and ADCS PCB's, which intelligently control those subsystems and communicate via the board backplane with the main OMAP processor via the I²C protocol, a standard two-wire serial protocol.

The OMAP5912 is a low power, high performance dual-core processor with an ARM9 32-bit microprocessor and TMS320C55x digital signal processor (DSP) in the same chip. The ARM9 is the central processing unit that hosts the Linux operating system, built on the 2.6 kernel, and associated device drivers. The flight software, developed at U of I, coordinates internal and external data operations, monitors spacecraft health, and collects, formats, and interfaces with the CubeSail control board, sending commands and storing data (photos). The DSP performs the required calculations for the attitude determination and control algorithms and serves as the terminal node controller/modem during satellite-earth communications, providing a data rate of 2400 baud, using a FSK modulation scheme. The capable DSP core in the OMAP5912 should allow other bandwidth efficient modulation schemes such as QPSK and QAM to be designed and implemented as required.

The communication system is based on a half-duplex amateur band radio (Dataradio DM-3475) tuned to ~437 MHz (the actual frequency is applied for though the FCC, coordinating with the ARC) with

variable 0.75-2 W transmit power. The radio is connected to the software TNC implemented in the DSP and the AX-25 protocol is used for uplink and downlink. A circularly-polarized, crossed dipole antenna has been constructed from a memory metal that is folded up against the satellite and is deployed using nichrome wire and monofilament. The antenna was designed to have a good omnidirectional pattern to ensure communication with the spacecraft regardless of the current attitude as shown in Fig. 15.

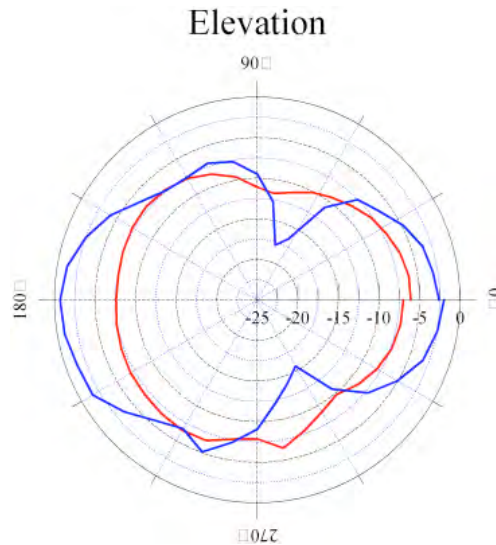


Figure 15: Beam pattern of crossed dipole antenna for uplink and downlink communication on TIWS, demonstrating its measured omnidirectionality.

ADCS SUBSYSTEM

IlliniSat-2 has full closed-loop three-axis attitude determination and control, implemented on board the spacecraft via a magnetic control system. An integrated high-precision low power 3-axis magnetometer (Honeywell HMC6343) and a coarse sun sensor are used for attitude determination. The information from the attitude sensors is fed into a Kalman filter (KF) for attitude estimation, yielding an attitude knowledge to within one degree per axis. The attitude estimate is passed through a linear quadratic regulator (LQR) to determine the optimal control input for the magnetic torque coils. Both the KF and LQR algorithms are to be implemented on the DSP. Magnetic torques are provided by torque coils fabricated on a flexible printed circuit made from a polyimide film (Kapton) that is integrated into the solar panels as shown in Fig. 16. The coils provide three-axes control, with redundant systems in the X and Y direction. In addition to providing the torque coil, the flexible circuits also provide power routing from the solar cells to the power board. Following P-POD deployment, the system will autonomously begin a detumbling procedure to reduce rotation rates to 0.1 deg/s and prepare the satellite for science and communication operations. After detumbling, the ADCS subsystem will maintain the attitude of the spacecraft to within five degrees to comply with the mission requirements.



Figure 16: Torque coil implemented on flexible printed circuit.

STRUCTURE AND THERMAL CONTROL SUBSYSTEM

The spacecraft structure uses a system of rails and plates. The rails connect the sections together and dictate the form factor of the satellite. The payload, separated from the bus by a middle plate, interfaces directly with the top plate and the satellite bus interfaces directly with the bottom plate.

Figure 14 demonstrates the solid model of the full satellite assembly. All the supporting system boards screw directly into the bottom plate, while the battery attaches to the middle plate. The solar panels are connected using six bolted joints, while their power harnesses attach directly to the power board in the stack. The payload is attached to the top plate. Power and data connections for the payload are provided via a wiring harness, accommodated by a channel in each of the bus PCB's and the center plate. The bottom plate serves as a radiator, so the selection of an appropriate optical coating can aid in the necessary thermal control. Heat from the PCB's and other components are conducted along embedded thermal planes to the standoffs, which then conduct the heat directly to the bottom plate. Heat from the batteries conducts through the middle plate, down the rails to the bottom plate, and heat from the payload is conducted down the rails to the radiating bottom plate.

Initial analysis has shown that the structure meets all mechanical requirements, and has previously passed a preliminary vibration test. The initial thermal models are promising, however additional simulation are required before the system is ready for a thermal vacuum test.

MISSION OPERATIONS, GROUND STATIONS, DATA DISTRIBUTION

The IlliniSat-2 radio transceiver is a commercially available data radio operating in the 70 cm band. An application will be filed with the FCC to obtain an amateur band "space station" frequency allocation and a pre-space notification will be made to the FCC no later than 90 days before integration with the launch vehicle according to 47 C.F.R. § 97.207 of the FCC rules. The amateur licensed frequency range in the 70 cm band allowed for "space stations" according to 47 C.F.R. § 97.207 is 435-438 MHz, all of which is accessible by our selected radio.

The satellite ground station was constructed several years ago in preparation for the launch of ION1. Students and staff have had great success contacting on-orbit amateur band satellites, and verifying proper station operation. The primary station radio is dual band 2 m/70 cm with enhanced satellite functionality (Icom IC-910H). Two high gain Yagi-Uda antennas (one for each band) are mounted on a

motorized elevation/azimuth rotator atop a 35-foot antenna tower on top of a four-story building on the Illinois campus. Commercially available satellite tracking software is used to determine overhead pass times and control azimuth and elevation rotators for the ground station antennas tracking the satellite. The software automatically calculates anticipated Doppler shift in the signal and tunes the radio appropriately.

TECHNOLOGICAL READINESS AND HERITAGE

Small satellites and payloads in the 1-2 kg class, called CubeSats, and 20-30 kg, called nanosats, have been under development at the University of Illinois since late 2001. The ION1 CubeSat was a 2U CubeSat with a photometric remote sensing instrument. ION1 was lost in the failed DNEPR launch attempt on July 26, 2006. The IlliniSat-2 development began in the fall of 2005, and primarily focused on the development of a new spacecraft bus and supporting equipment. The University of Illinois has also continued work on additional payloads, and partnered with Taylor University on other remote sensing payloads for the TEST Nanosat. Faculty program direction is provided by G. Swenson and V. Coverstone who oversee and provide guidance for the spacecraft bus development.

The past several years have been dedicated to the development of the IlliniSat-2 bus, which is near completion. First revision PCB's are nearly prepared for manufacture and the spacecraft structure is mature, machined, and has completed a first round of vibration testing.

GROUND FACILITIES

The University of Illinois currently has two laboratories for CubeSat development and testing. A hardware lab with 4 electronics workstations, soldering facilities, a Class 10,000 clean room, a thermal vacuum chamber, and a magnetic test facility are dedicated to hardware design and testing. A software development/modeling lab has an additional seven computer workstations equipped with advanced engineering software packages, provided by the College of Engineering. General software tools available include compilers and development environments, MATLAB, Pro/Engineer, Unigraphics, NX Space Thermal, and EagleCAD for hardware and software simulation and verification. Should the need arise, the project also has access to cluster computing to handle the larger simulations and analysis.

The Illinois CubeSat program has an operating ground station for tracking and communicating with the 430-MHz frequencies. Many of our team members are active in the amateur radio community and have the required licenses of operating frequencies needed for ION1 operations. Since a standard amateur radio packet system is being used, the world-wide amateur radio community can be involved in the monitoring of the spacecraft. In addition, the ground system is fully controllable via the Internet, for those granted access privileges. This level of accessibility allows students the potential opportunity to partner with student groups at other universities around the world for satellite operations, and increase the daily window of opportunity for satellite communication.

PAYLOAD DESIGN, REEL AND SLIT

The payload design for CubeSail consists of three main components: the film reels, the separation release unit (SRU), and the camera. The reel assembly, Fig. 17, must fit within a 90 mm x 90 mm x 84 mm payload volume. The width of the bobbin within the flanges is 81 mm and the film width is 77 mm to allow for 2.0 mm separation between the film and the flange.

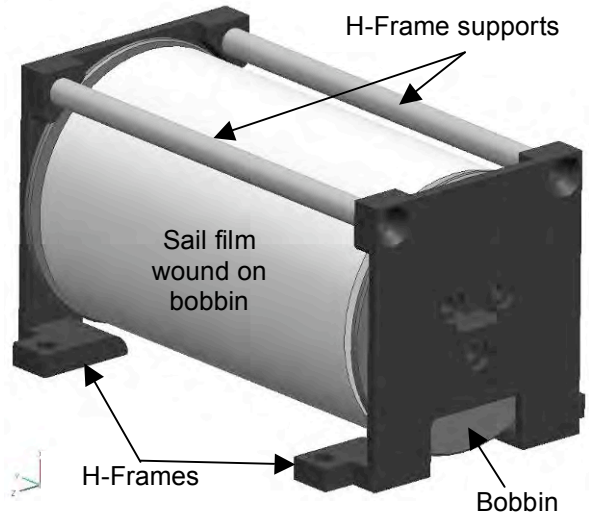


Figure 17: Bobbin design.

As shown in Fig. 18, the bobbin assembly includes two open bearings and a motor assembly.

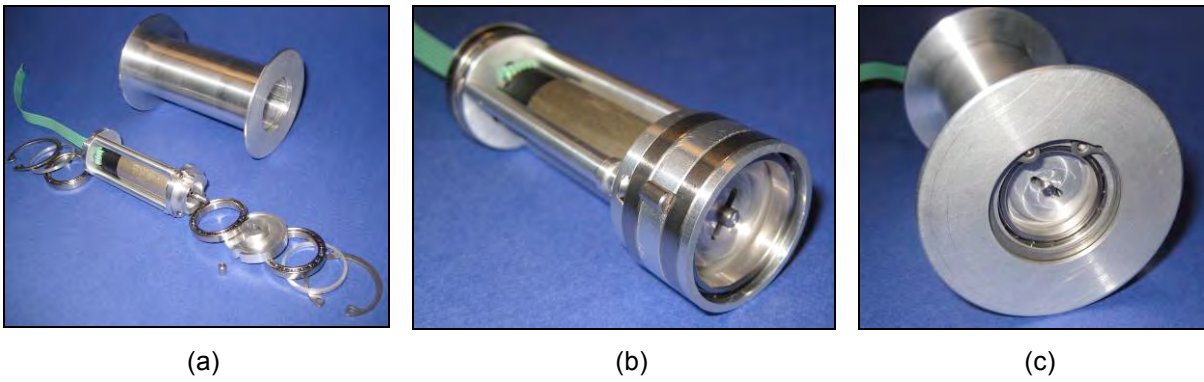


Figure 18: Bobbin hardware components – (a) separated, (b) assembled, (c) installed.

A wound bobbin is shown below in Fig. 19. Note that there is a gap between both flanges and the film, Fig. 20, as during testing it was determined that film unwinding was impeded when the sail material touched the flange/edge of the bobbin.

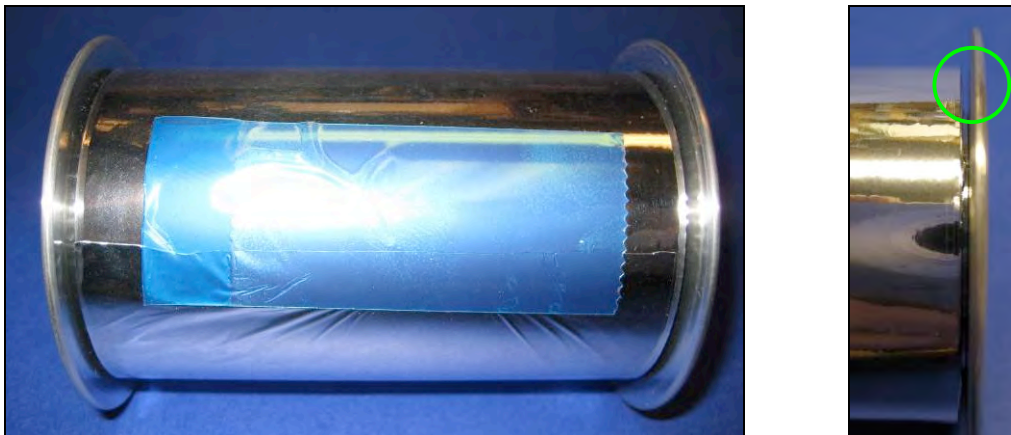


Figure 19: Aluminized Mylar® film wound on bobbin.

Figure 20: Clearance between film and flange.

SEPARATION RELEASE UNIT (SRU)

The two CubeSats, A and B, are launched as a single unit, and must be separated in orbit after ejection from the booster. This is accomplished with a Separation Release Unit (SRU), which is based on release technology previously employed on CubeSats. The baseline design called for 2 SRUs, straddling the film slit, with a mass budget of 50 g for 2 SRUs.

A mechanical simulation experiment called the Bearing Rail experiment (BRE) is being developed to test the Separation Release Unit (SRU) (Figs. 21 – 24). Each CubeSat is suspended from a linear ball bearing with the sail film extending between them, Fig. 21. The linear bearings slide along a 1-m hardened steel rod. The far end of each rod is attached to a linear translation stage which allows independent downward alignment of the far end of the rods such that friction can be canceled by gravity and the satellites will separate at a constant rate. Calculations were performed to find the optimal diameter of the rod such that there is less than 0.1 mm deflection caused by the weight of the cubesats along the 1 m length; that diameter is 0.75". The satellites are attached to a yoke assembly via a pivot bearing which allows pitching motion and then attached to the linear bearing via another pivot bearing which allows yaw motion. Balance weights are used to bring the mass to ≈ 2 kg per satellite, with the c.g. near the CubeSat geometric center.

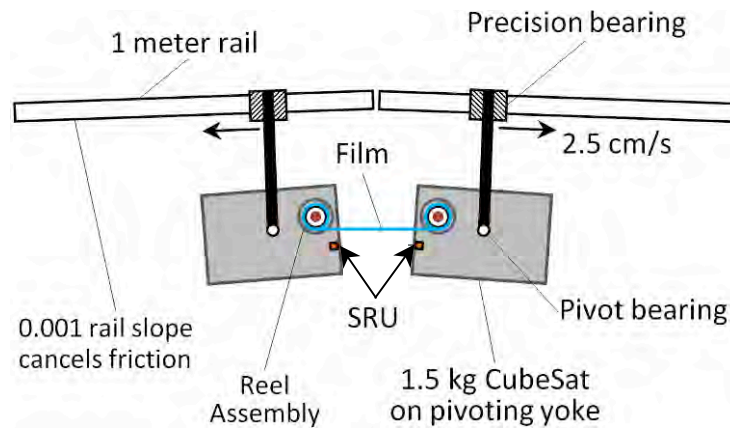


Figure 21: Bearing rail experiment.

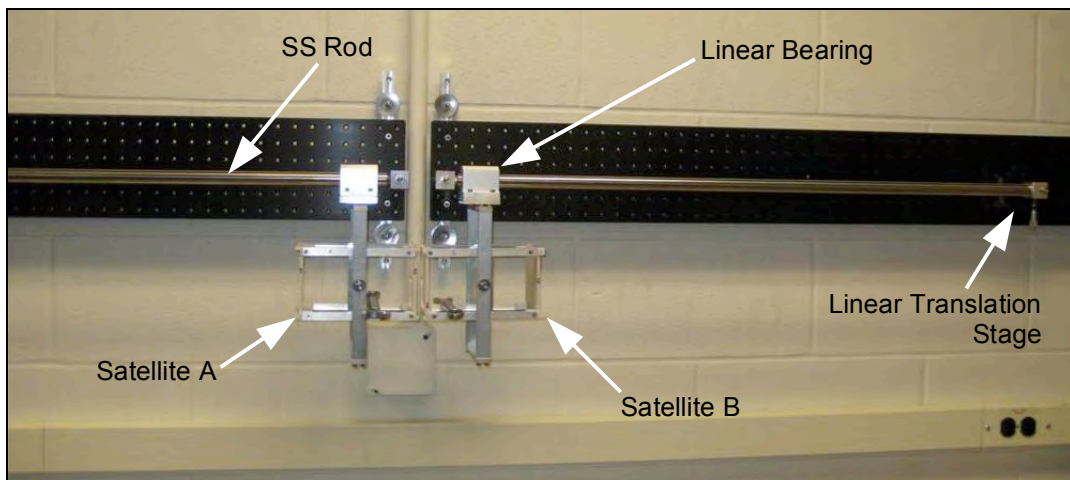


Figure 22: Bearing rail experiment mounted to lab wall.



Figure 23: BRE, end view.

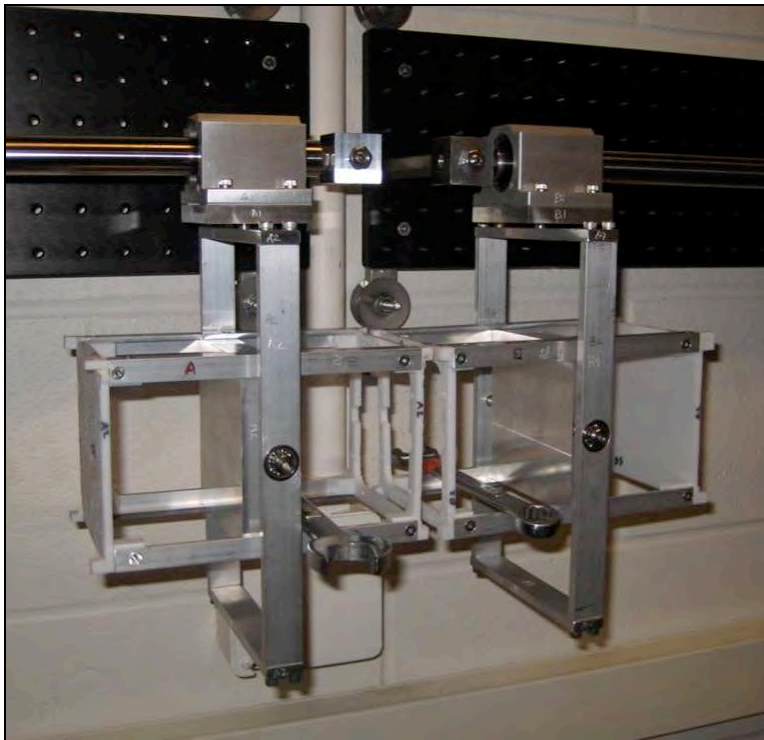


Figure 24: Bearing Rail Experiment.

The SRU is under development. A TiNi Aerospace shape memory alloy pinpuller device had been evaluated, but it was decided that an SRU would have to be designed.

SATELLITE RELEASE MECHANISMS

The baseline SRU design called for the separation springs for the two spacecraft to be secured and held in place with a monofilament, held in close contact with a short length piece of small-diameter nichrome wire. When ready for deployment, current would be passed through the nichrome wire, heating and melting the monofilament, releasing the springs. This method has been used in the CubeSat community for antenna deployment for some time, and is so used on the Illinois CubeSat.

During launch and at booster ejection, the film, which is located between the two connected satellites, is kept at a low-level of tension. The separation scenario is: a) the SRU wire is heated, breaking the SRU; b) the reel motors are started at a predetermined rate, e.g. 1 cm/s; c) the springs provide a separating force, and d) separation velocity is maintained by the speed of the motors. The SRU and its spring are designed with respect to the center of gravity (CG) so as to minimize rotational torque on CubeSats A and B. Once separated sufficiently, film tension is maintained either by spin- or gravity-gradient stabilization.

A second approach was based on the tensile failure of heated Nitinol shape memory alloy, as shown schematically in Fig. 25. This approach had high power consumption, and was difficult to assemble.

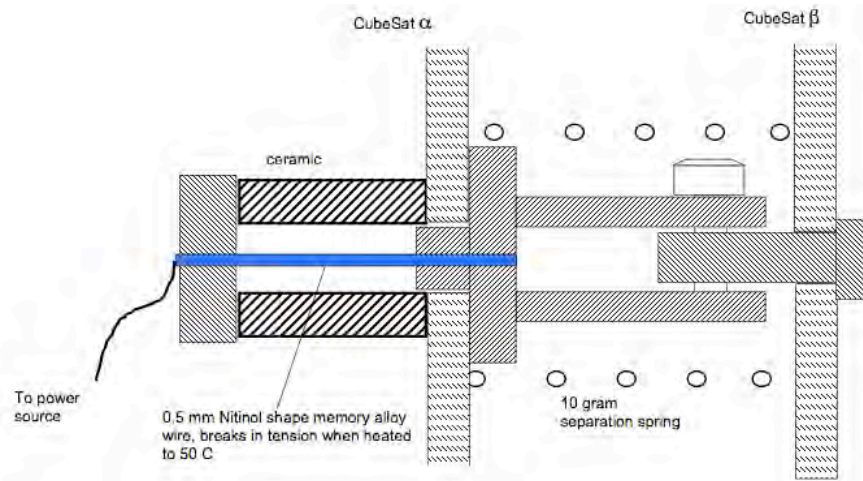


Figure 25: CubeSat Nitinol separation release unit.

A third approach to the separation release unit (SRU) design, consisted of a 12 V solenoid, mounting hardware, latching pin, microprocessor for solenoid activation, and switching device, Figs. 26 and 27. Prior to the hardware being installed in the satellites, the solenoid was bench-tested with the SRU hardware and RC circuitry and deemed to be functional and adequate for initial BRE testing.

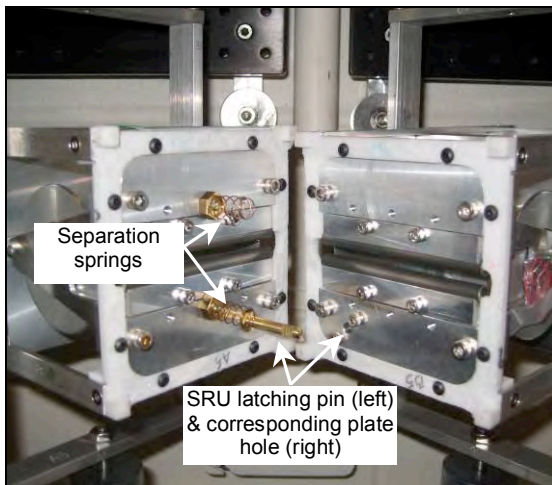


Figure 26: SRU installed.

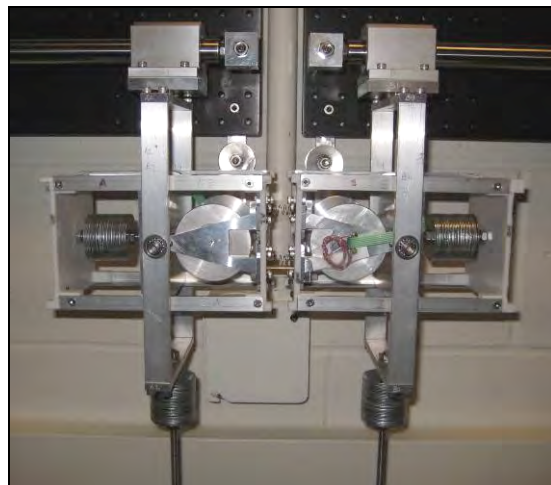


Figure 27: BRE with reel assemblies installed; balanced.

Three primary versions of the solenoid separation release unit (SRU) are shown in Fig. 28. The first generation (Fig. 28a) had tolerances that were too large. The second generation (Fig. 28b) had tighter tolerances, but resulted in too much friction between the pins which impeded retraction of the solenoid pin. The third generation conical design (Fig. 28c) caused tipping of the two satellites resulting in friction between the SRU pin and the sleeve bearing. Because of the problems associated with the solenoid SRU, another SRU concept has been implemented, the motor SRU.

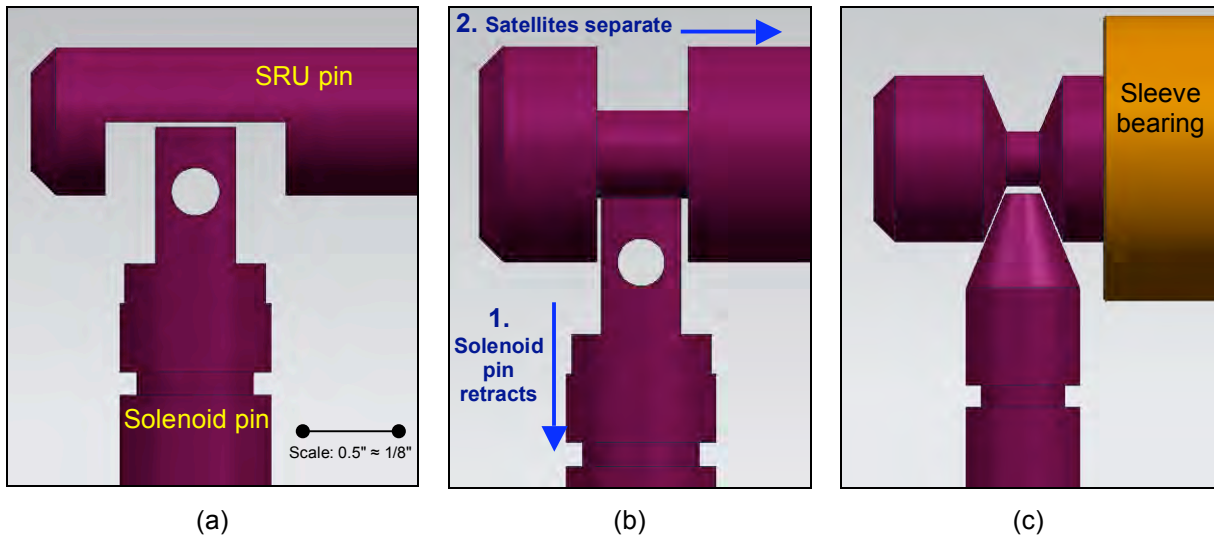


Figure 28: Design progression and separation steps of the SRU and solenoid pins.

The current generation SRU consists of a lead screw and gear motor (the same as used in the sail film bobbins) on one payload plate and a threaded hole mounted to the other payload plate, Fig. 29. The motor is remotely controlled to turn the lead screw pinned to its shaft, which then unscrews from the threaded hole. As the lead screw turns out of the hole, the separation springs push the two satellites apart.

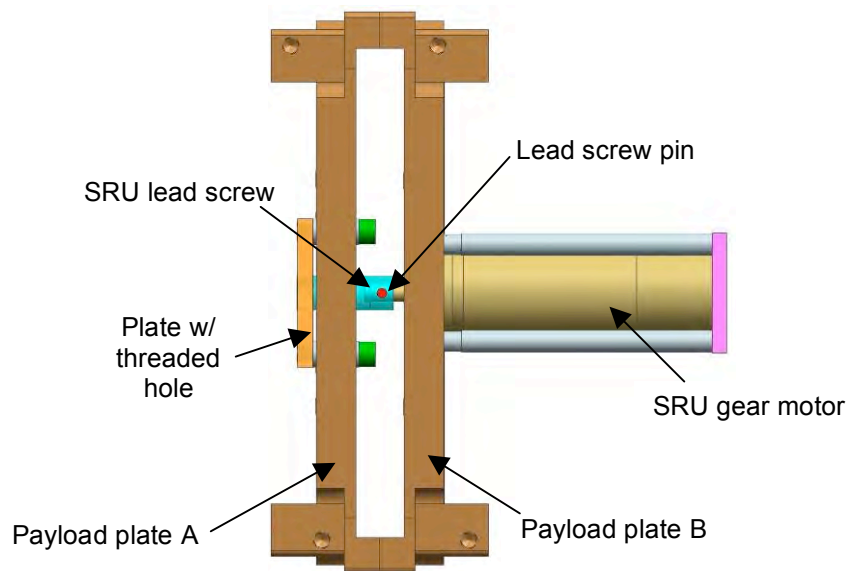


Figure 29: Motor SRU concept.

The separation springs were chosen based on a desired separation speed of 5 – 10 cm/s. Figure 30 shows a drawing of the payload plate with holes for the separation springs. The locations were chosen to be as close to the slit as possible to impart a minimum moment from unequal springs. The optimal number of springs will be determined through experimentation on the BRE.

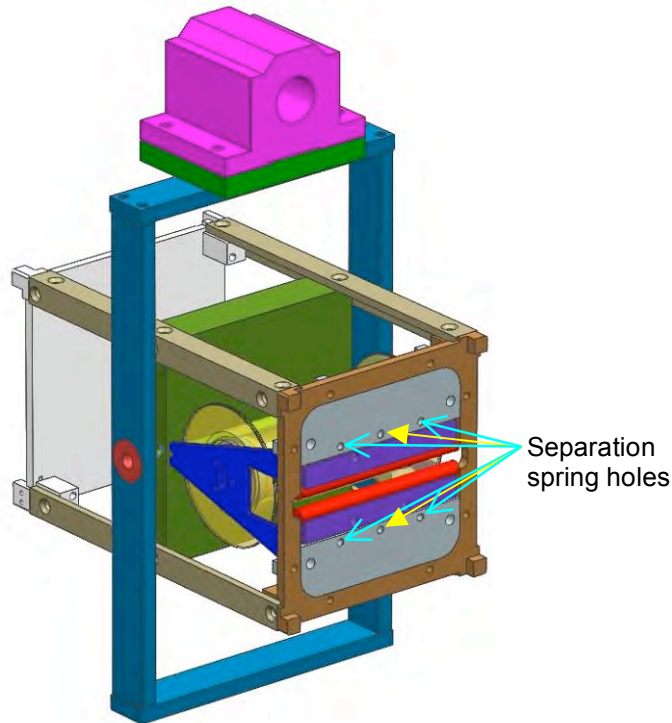


Figure 30: Satellite payload plate with separation spring holes noted.

SRU CONTROL SYSTEM

The CubeSail SRU separation sequence uses two feedback sensors that accurately monitor the position of both the screw and the bobbin motor. The sensors, together with a 16-bit microcontroller, a DC motor controller, and H-bridge switches, make the following requirements of the control system possible:

1. The motor shaft of the screw motor does not stall when initially separating the satellites.
2. The screw motor rotates at 24 RPM and the bobbin motors in each CubeSat release the sail film at 5 cm/s.
3. Unexpected frictional forces of the motor shaft with any other component of the satellites are rejected. Unexpected frictional forces affecting the rotating shaft are compensated for by increasing motor torque to keep velocity constant.

To avoid stalling of the gear motor when it starts unscrewing, the SRU is unscrewed with at least three times the installed torque. The factor of three overcomes frictional forces when initially separating the satellites. The target speed and position of the motors is met by using PID controllers, which compensate for frictional forces that the rotating components might have against the satellite structure.

The separation sequence is commanded by the microcontroller, as follows:

1. The film is unwound by the amount slightly longer than the distance of the SRU lead screw stroke.
2. The gear motor starts separating the satellites until it completely disengages from the other satellite, leaving the film in tension, produced by the separation springs.
3. The bobbin motors then separate the satellites at 10 cm/s from each other.

The microcontroller also accepts commands in an event where manual input is required.

The circuitry to control the SRU, called the Radio Controlled Open Loop Controller (RCOLC), is shown in Figs. 31 – 33 and Table 3.

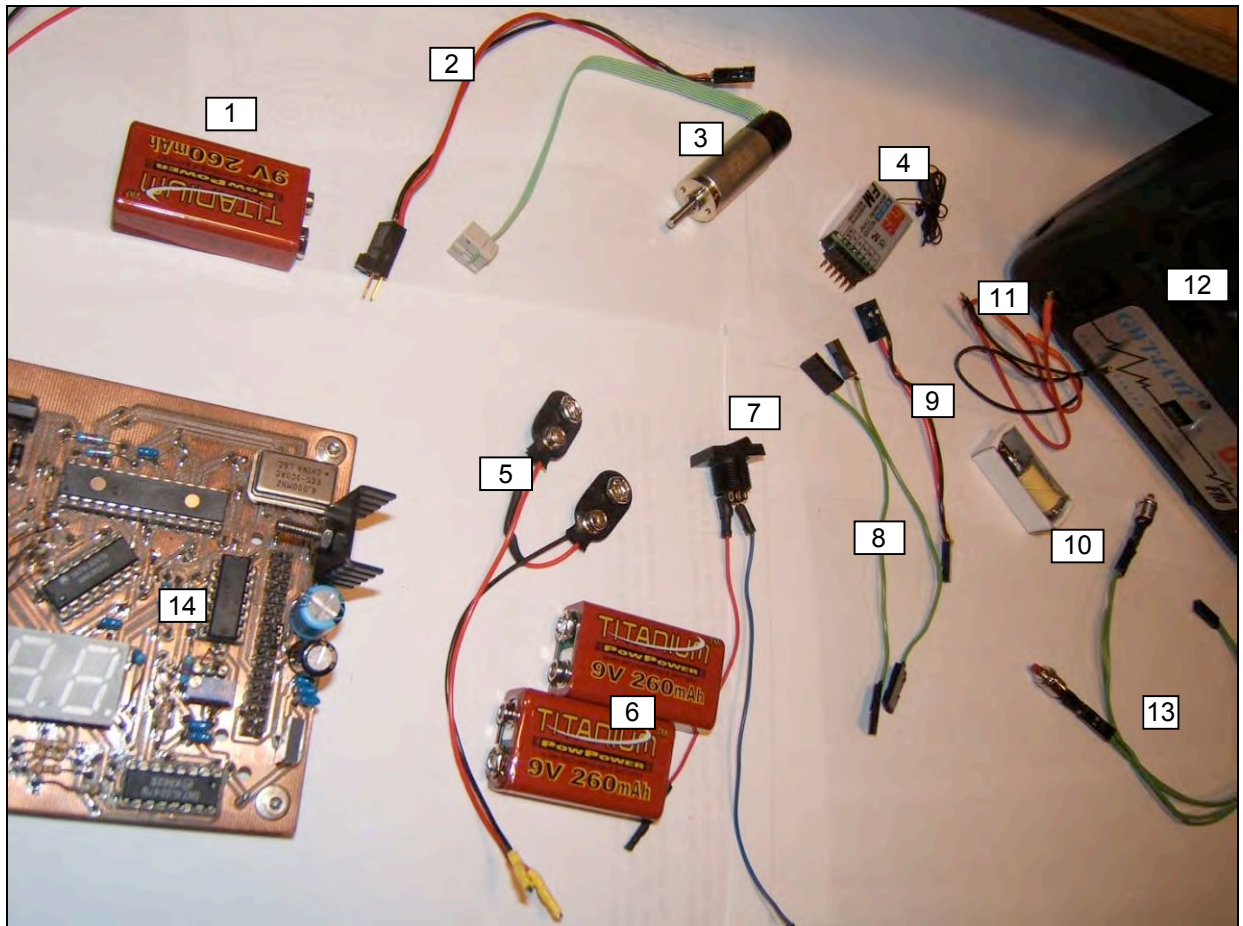


Figure 31: RCOLC components.

Table 3: RCOLC components list.

#	Description	#	Description
1	SRU battery	8	Radio data harness
2	Motor harness for connecting motor with PCB	9	Radio receiver power harness
3	Motor for bobbin	10	Solenoid SRU active component
4	Radio control receiver	11	Solenoid connectors
5	9 V battery in-series connector for main power	12	Radio controller
6	9 V batteries for main power, 2x	13	Push buttons, 2x
7	Main power switch	14	PCB with open loop motor control radio receiver, and SRU activation capabilities.

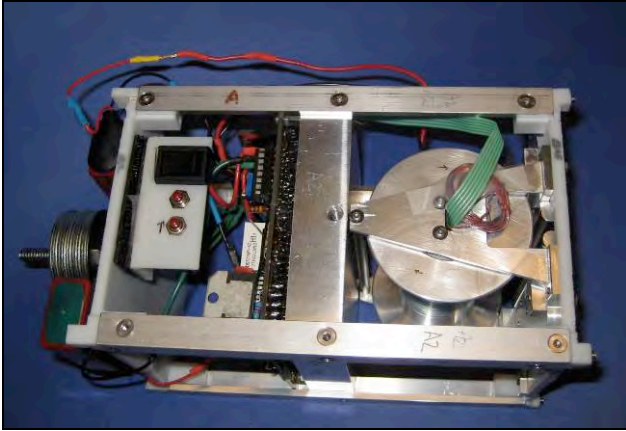


Figure 32: Satellite A with PCB installed.

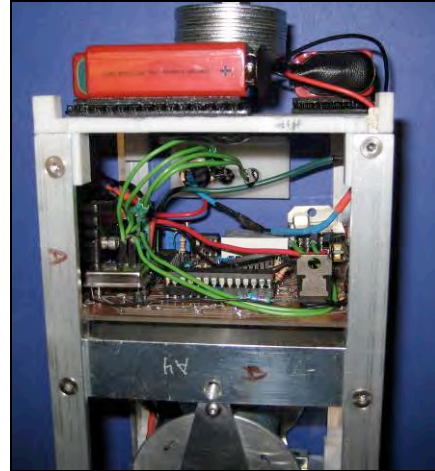


Figure 33: Close-up of Satellite A, PCB installed.

CAMERA

As part of the payload, one camera on each satellite is used to observe the film as it unreels, as well as the satellites as they separate from each other. Experiments were performed in the lab with the objective of determining the picture clarity and visibility from the lens of the satellite camera. An ordinary cell phone camera was used to help simulate the resolution qualities expected from the satellite camera, since they share similar characteristics (Table 4 and Fig. 34).

Table 4: Camera comparison.

	Cell Phone Camera	Satellite Camera
Manufacturer	Sony Ericsson	Electronics123.com
Model	w300i	C328R
Sensor	CMOS	CMOS
Resolution	VGA 640x480 pixels	VGA 640x480 pixels
Color	Color/Monochrome	Color/Monochrome



Figure 34: C328R Mini CMOS camera.

To simulate the twisting that may occur in space, pictures were taken at various angles rotated from 0° - 90° . This angle would be measured relative to the rotation of the two CubeSats. It was difficult to keep the sail surface smooth, but the pictures were adequate for the purposes of the experiment (Figs. 35 – 36).

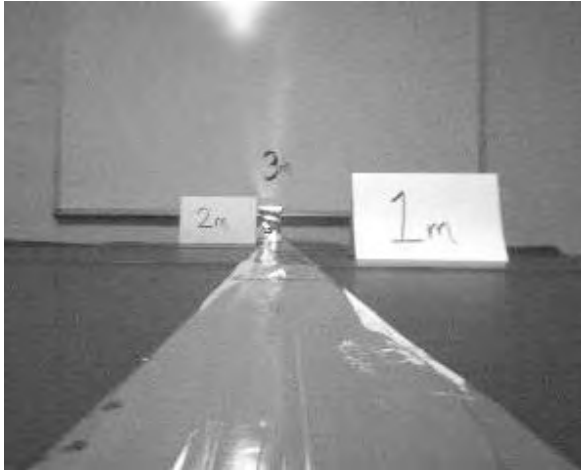


Figure 35: Rotated 0° .

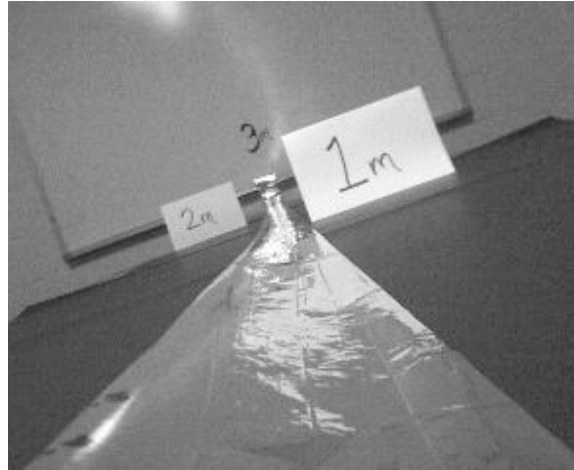


Figure 36: Rotated 30° .

DETUMBLING AND RE-ORIENTATION OF THE CUBESAIL ASSEMBLY

The separation of the spacecraft from the upper stage of the launch vehicle will impart residual torques onto the spacecraft, resulting in non-nominal attitude and potential three-axis tumble. Before the sail deployment can begin, the combined CubeSail assembly must be de-spun and oriented with its long axis along the local vertical direction. In practice, it is difficult to accurately predict the spacecraft's initial attitude and rotational rates *a priori*, requiring a robust controller that is capable of handling a wide range of initial conditions.

Historically, the final stage and the P-POD for a CubeSat-class spacecraft impart at most 2.5 deg./sec angular velocity to all three axes. Since initial despinning and stabilization of the CubeSail is critical to mission success, the controller is designed with 100% margin and is capable of handling 5 deg./sec rotational rates on all three axes.

CubeSail attitude control is accomplished with three-axis, variable-strength magnetic torquers. The actuators consist of a novel design that imprints consecutive copper loops in a wind-down pattern on a flexible circuit board, four layers deep, shown previously in Figure 16. The flexible torquers are mounted behind the solar panels, include all necessary control circuitry, and are capable of producing maximum magnetic dipole moments of $0.106 \text{ A}\cdot\text{m}^2$ (at $i_{\text{max}} = 0.4 \text{ A}$). Since both satellites have identical attitude control capability and the torquers can be fired simultaneously, the initial detumbling and stabilization can be accomplished using a maximum dipole moment of $0.212 \text{ A}\cdot\text{m}^2$.

The control problem is formulated using Linear Quadratic Regulator theory [Bryson, 1975][Brogan, 1991][Psiaki, 2001]. The desired performance of the system—in terms of power consumption and stabilization time—is achieved by appropriate selection of the cost function and two weight matrices, Q and R. In practice, selection of appropriate Q and R matrices (9x9 and 3x3 diagonal matrices respectively) that yield robust results for a given orbit and a wide range of initial conditions is very difficult. In order to allow easy adjustment to these matrices and evaluation of their performance, a Matlab-based simulation that incorporates CubeSail system dynamics, models for the magnetic field, aerodynamic drag, and gravity gradient, as well as LQR control theory has been developed. The simulation is used in conjunction with a simple Genetic Algorithm (GA) [Goldberg, 1989][Pukniel, 2006] to find a near-optimal set of Q and R matrices to minimize a despinning and orientation times, while not exceeding available power limits.

The results presented below are sample simulation outputs based on the following assumptions. The spacecraft was assumed to be a rigid body with the dimension of 30x10x10 cm and mass of 3 kg. At this time, the center of mass was assumed to coincide perfectly with the geometrical center of the two-satellite assembly. This is seen as an acceptable assumption since the CubeSat Design Specification requires them to be within 20 mm of each other. Moreover, a parameter that represents any such deviation is incorporated in the simulation code and is used in the aerodynamic torque calculations.

The spacecraft was assumed to be inserted into a typical CubeSat orbit, here assumed to be a 750 km altitude circular low Earth orbit inclined at 98°. The orbit was propagated for 15 hours and included gravity gradient and aerodynamic drag disturbance torques, as well as the applied magnetic control torque. The coefficient of drag was chosen to be 2.2 and the aerodynamic density was chosen to be the mean of solar maximum and solar minimum densities at 750 km, or $4.5 \times 10^{-14} \text{ kg/m}^3$. The atmospheric density values were calculated using the NRLMSISE2000 code.

In order to evaluate the robustness of the controller for various orbital deployment scenarios, the simulation was run 1000 times with randomly generated initial attitudes. All simulations assumed the worst-case scenario with initial rotational rate of 5 deg./sec on all three axes. Figures 37 and 38 are a representative sample of the output from a single run.

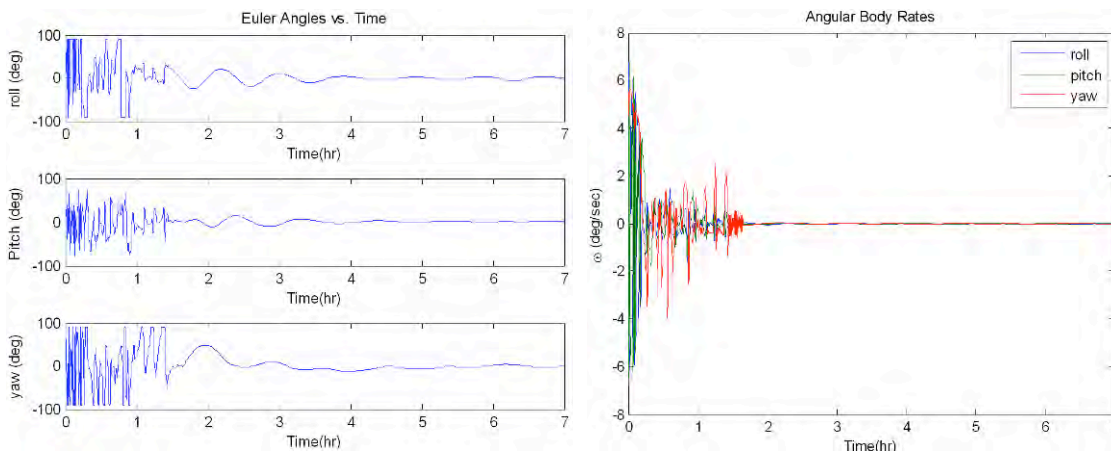


Figure 37: Euler angle history (left) and angular body rates (right).

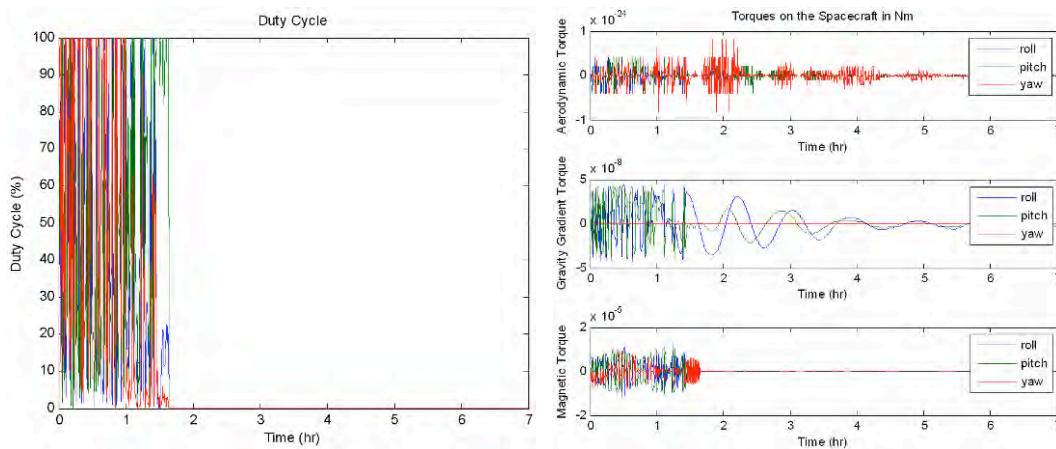


Figure 38: Duty cycle history (left) and torques on the spacecraft (right).

As can be seen in Fig. 37 (left), the spacecraft is stabilized in approximately 2 hours. The rotational rates are reduced to under 1 deg./sec in 0.5 hours and further reduced to near zero in the next 1.5 hours as seen in Fig. 37 (right). Figure 38 (left) shows that the controller initially used almost 100% of available torque authority to reduce the rotational rates and then used finer control to achieve the nadir-pointing attitude. The torques applied to the spacecraft, which include magnetic, aerodynamic, and gravity gradient, are shown in Fig. 38 on the right. It is worth pointing out that prior to sail deployment, the drag force is nearly negligible. This is due to the assumption that center of mass is aligned with the geometrical center, causing the center of gravity and center of pressure to coincide and produce no torque.

DEPLOYMENT ANALYSIS

Preliminary analysis of the CubeSail deployment methods yielded two viable options, shown in Fig. 39. In the spin-induced deployment method, shown on the left, the mated satellites are spun together using onboard magnetic torquers and then released by engaging the SRU. The film is unwound until the rotational rate of the system decreases to a prescribed threshold level that ensures the film does not billow out excessively. At this time, the tip satellites rotate in opposite directions along the long axis of each spacecraft, inducing a twist in the film. If properly oriented relative to the sun, the resultant pitch in the blade forces the system to act as a 'propeller' and spin up. Once the desired rotational velocity is achieved, the satellites return to their zero-pitch attitude and more film is unwound. This process is repeated until the final spin rate and deployment length are achieved.

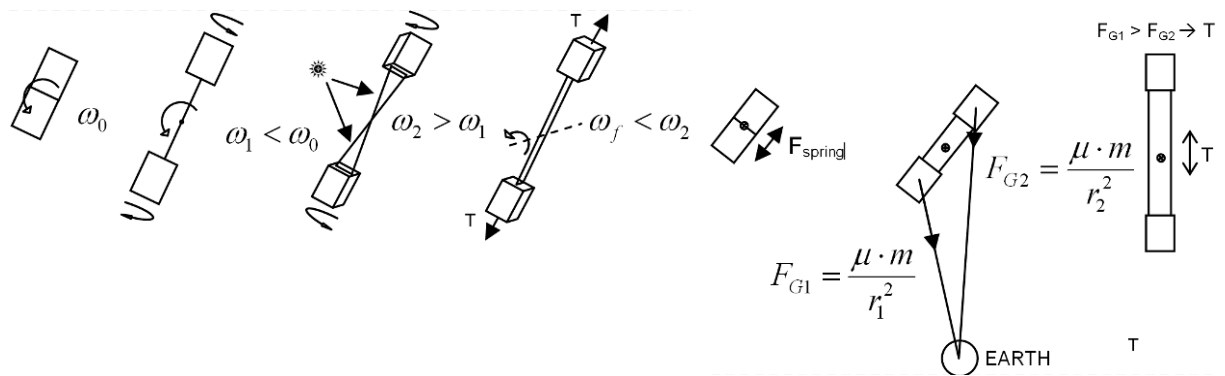


Figure 39: Sail Deployment Options: Spinning (left) and Gravity Gradient (right).

The centrifugal force of the rotating system provides the tension necessary to keep the film relatively flat. The challenge of this approach resides in the complicated dynamics of two rotating CubeSats connected by a non-rigid tether. Due to the limited responsiveness of the attitude control system, this deployment method is reserved for a second CubeSail demonstration, after deployment hardware and various other subsystems have been space qualified.

The second deployment method, shown on the right side of Fig. 39, utilizes gravity gradient force between the two CubeSats to provide the necessary tension in the film. The mated satellites are oriented into a nadir pointing attitude and separated using two compressed springs. The spring constants are selected by modeling the dynamical behavior of the two satellites during deployment and imposing a final boundary condition of zero relative velocity and zero displacement away from the local vertical. The initial conditions assume the spacecraft are aligned along the local vertical resulting in one free variable, the radial separation velocity, which is solved for numerically and then correlated to an appropriate spring constant through the principle of conservation of energy.

The film is unwound using the reel motors until the entire sail length is deployed at which point the gravity gradient force provides the desired tension. Fortunately, the rate of solar pressure force increases at the same rate as the gravity gradient force and is equal to approximately five times the desired value. There are several advantages to using the gravity gradient method, including: simplified deployment dynamics (no spin-up maneuvers or complicated dynamics associated with rotating spacecraft), passive attitude stabilization of the system, and overall mission risk reduction.

Preliminary analysis of the gravity gradient deployment dynamics of a 260 m film has been performed for a spacecraft in an ecliptic orbit. The ecliptic orbit offered a relatively disturbance-free environment, in which a sail flying with its edge to the velocity vector experienced minimal aerodynamic drag and minimal solar radiation pressure forces. As such, it was initially selected as a candidate CubeSail orbit, but due to non-constant lighting conditions has been eliminated in favor of the sun synchronous terminator orbit. The non-linear equations of orbital motion were solved numerically to meet final boundary condition of zero deviation away from nadir and zero relative velocity. The initial boundary condition assumed a perfectly nadir oriented spacecraft and an initial separation velocity in the radial direction, the latter of which is a free variable.

Figure 40 shows the results of the integration, where l and \dot{l} represent the deployed sail length and length rate and θ and ϕ represent in-plane and out-of-plane angles in the orbital frame. The deployment is accomplished in approximately 1.3 hours and meets both boundary conditions with the initial separation velocity of 0.175 m/s.

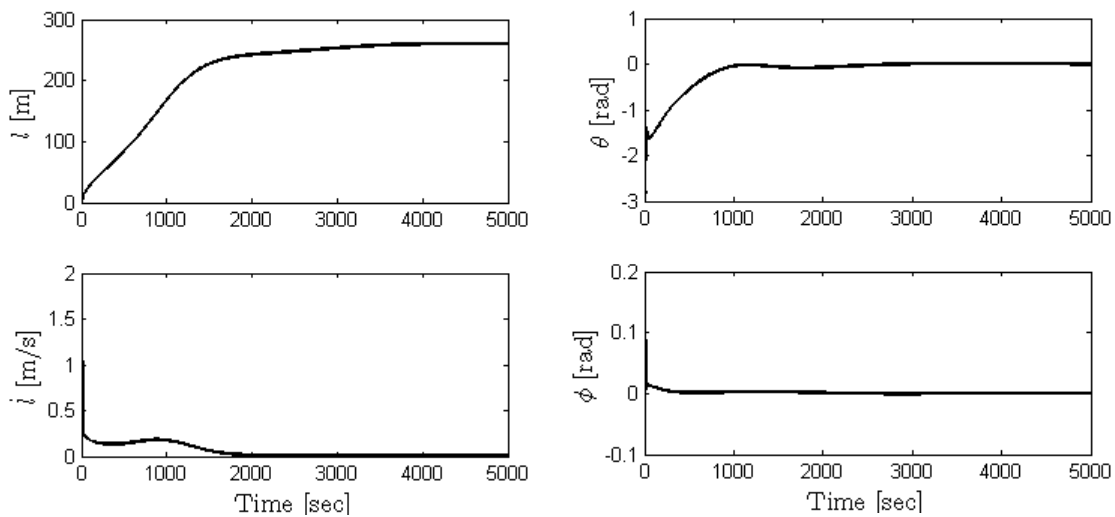


Figure 40: Gravity gradient deployment dynamics.

The gravity gradient deployment demonstration is seen as an opportunity to test several of the CubeSail subsystems, including magnetic torque actuation hardware and LQR performance, reel assembly and motor, sail dynamical models, reaction wheel control (discussed shortly), camera performance, and several bus subsystems. Validation of performance of these subsystems and any consequent re-designs would pave the way for a more complex demonstration of the spin-induced deployment and operations. This second demonstration would be a scaled-down version of the UltraSail mission and would test control methods and performance of fully rotating system, a main attribute of the UltraSail design.

ORBITAL MANEUVERS

The final phase of the CubeSail mission is the demonstration of propulsive capability using solar radiation pressure. In order to achieve the desired thrust direction, the tip satellites are pitched in opposite direction, inducing a twist in the film. The transfer maneuvers typically last several hours or days (depending on available power), necessitating a fine control authority to maintain the desired pitch angle in the presence of disturbing torques from aerodynamic drag and solar radiation pressure. Solving the optimal control problem for magnetic torquers during orbital maneuvering is not only computationally and power intensive, but also difficult to execute accurately due to dependence on a continuously varying external magnetic field. As a result, pitching maneuvers necessary to maintain proper relative twist in the film may have to be accomplished with miniature reaction wheels. Each CubeSail tip satellite would use a single 10 mN-m-sec reaction wheel [Sinclair Interplanetary, 2009] (Fig. 41) to control the pitch angle.

The magnetic torquers would be used to dump momentum when the wheels become saturated or to remove momentum bias.

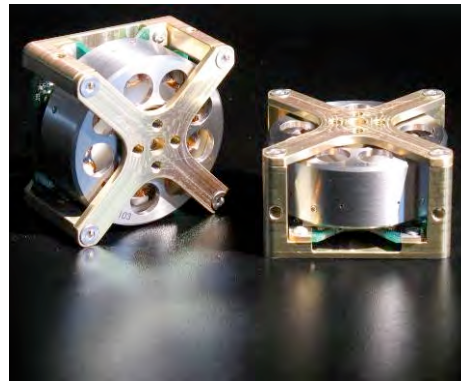


Figure 41: Sinclair Interplanetary 10 mN-m-sec reaction wheel.

In order to predict environmental effects accurately on the CubeSail spacecraft from initial deployment through nominal operations and orbital maneuvering, accurate force models have been developed. The solar radiation pressure model includes non-ideal sail effects from reflection, absorption, and re-radiation with the optical parameters listed in Table 5 [McInnes, 1999][Rowe, 1978][Wright, 1992][Wie, 2004].

Table 5: Optical coefficient of sample solar sails.

	\tilde{r}	s	ϵ_f	ϵ_b	B_f	B_b
CubeSail	0.88	0.94	0.05	0.55	0.79	0.55

The notation in the above table is as follows: \tilde{r} is the coefficient of reflection, s is the fraction of specularly reflected molecules, ϵ_f and ϵ_b are the front and back emissivity coefficients respectively, while B_f and B_b are fractions of molecules that reflect in a semi-diffuse fashion from the front and back surfaces respectively.

The aerodynamic drag model is based on the method of accommodation coefficients [NASA, 1971][Gaposchkin, 1994][Hughes, 1986] and takes into account interaction between the residual atmospheric constituents and the sail surface. Factors that affect this interaction include angle of attack, type and density of major atmospheric constituents at the desired altitude, orbital velocity, surface temperature and level of thermal accommodation of impinging molecules, and fraction of molecules reflected in the specular versus diffuse fashion. Sample calculations at an altitude of 800 km show that depending on the angle of incidence, α^{AD} , the equivalent coefficient of drag, $C_D^{Equivalent}$, varies between 2.85 and 1.35—a significant departure from the historically-used value of 2.2. $C_D^{Equivalent}$ is computed by equating aerodynamic drag forces computed using the accommodation coefficient method and classical drag equation.

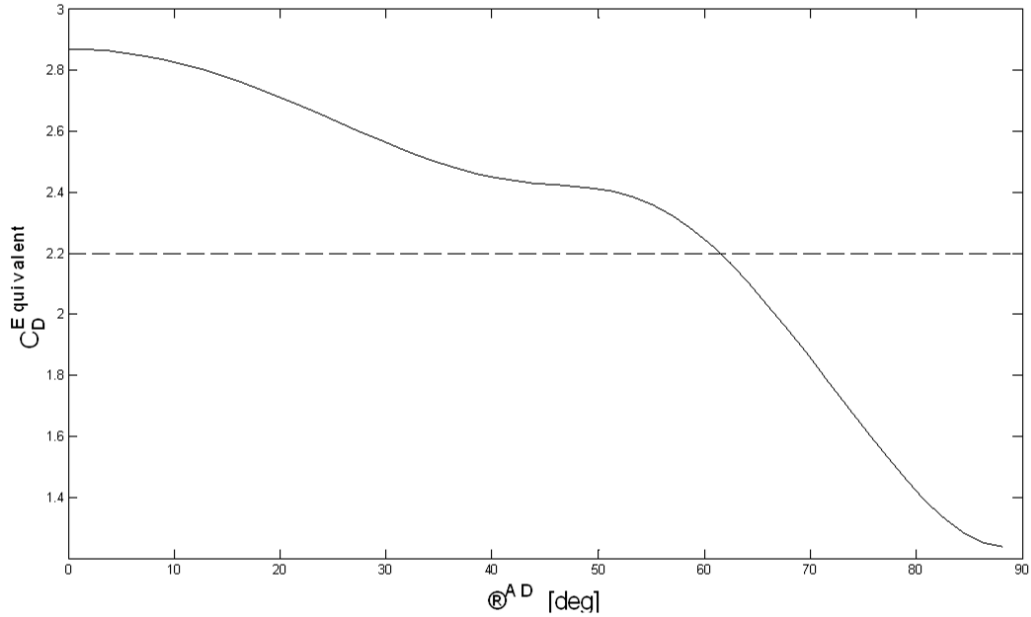


Figure 12: $C_D^{Equivalent}$ obtained by matching aerodynamic forces computed using accommodation coefficients and constant $C_D = 2.2$.

The above models are used in conjunction with the Edelbaum low-thrust orbit transfer theory [Chobotov, 2002][Edelbaum, 1961][Edelbaum, 1962] to compute transfer trajectories for three sample cases. The cases are summarized in Table 6 and include: 1) 100 km altitude raise with minimal inclination change (0.4° to maintain the sun-synchronous orbit), 2) 5° inclination change, and 3) 100 km altitude increase combined with a 5° inclination change. The results indicate that even modest inclination changes require long transfer times caused by minimal film area and hence available thrust. Time histories of velocity, inclination, and altitude for the third orbital maneuver case are shown Fig. 43.

Table 6: Summary of results of 3 orbital maneuvers.

Scenario	Δi ($^\circ$)	Δalt (km)	Transfer time (days)
(1)	0.4	100	69
(2)	5	0	333
(3)	5	100	322

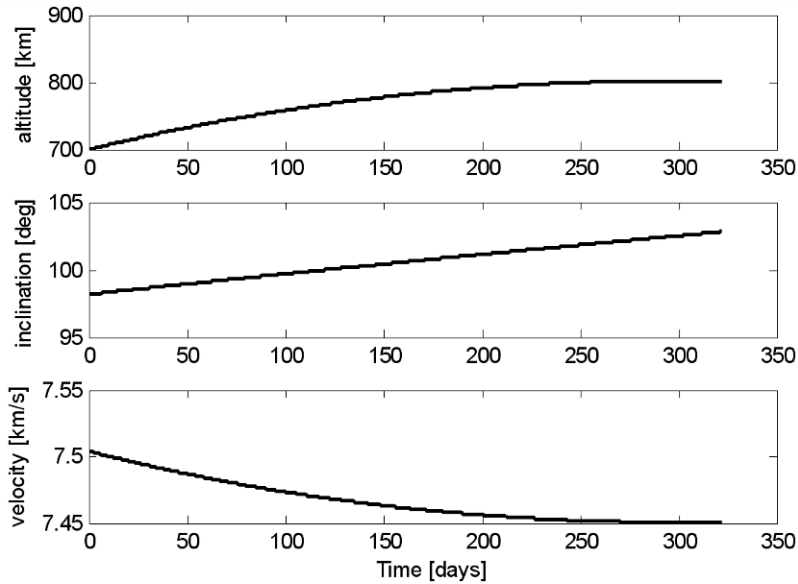


Figure 43: Time history of orbital maneuvers.

SPACECRAFT CHARGING

Spacecraft charging occurs as a result of the fact that at a given temperature, the electrons have a much higher velocity than do the ions, and a potential bias builds up on spacecraft surfaces. This is a well studied problem at geostationary orbit altitudes, and lesser so at LEO. A relevant study is described from charging events and anomalies on DMSP F13 spacecraft by Anderson and Coons [Anderson, 1996], for a satellite where unusual anomalies were experienced at 800 km. For the nominal ionospheric densities, surface charging to a few volts is not unusual. The amount of charge collected is related to the amount of conducted material exposed to the environment. For the DMSP F13 spacecraft, the high latitude exposure to the auroral ionosphere caused an anomalous condition of very large potentials (100s of Volts), which lead to discharge(s). In the case of DMSP, electron fluxes were nominally $<10^5 \text{ cm}^{-2}\text{s}^{-1}$, but exceeded $10^8 \text{ cm}^{-2}\text{s}^{-1}$ for periods of aurorally enhanced ionospheric exposure.

Spacecraft charging will be an issue to deal with. The deployed 20 m^2 area of an active conductor will be a very effective charged material regardless of direction to ram. For nominal ionospheric densities, charging potentials would be larger than those of DMSP, and for enhanced ionospheres, CubeSail would experience similar charging on its conductive film as well as to whatever the film is attached. Discharging of charged surfaces could lead to single event upsets as well as potential component failure.

SUMMARY AND CONCLUSIONS

UltraSail has been proposed as a controllable way to deploy and fly very large solar sails and the concept appears scalable. A pair of CubeSat nanosatellites are being assembled to deploy and fly a 20 m^2 sail as a low-cost technology demonstration in low Earth orbit. Modeling suggests that a gravity-gradient deployment is the best option, and laboratory experiments are being used to support the design.

ACKNOWLEDGMENTS

This effort is performed under NASA Contract NNX09CB37C. Les Johnson of NASA Marshall Spaceflight Center is the contract monitor. We also wish to acknowledge important technical discussions on sail film technology with Greg Farmer and Mark Johnson at NeXolve, Inc., Huntsville, AL.

REFERENCES

Anderson, P. C. and Coons, H. C., **Spacecraft Charging Anomaly on a Low-Altitude Satellite in Aurora**, J. Spacecraft and Rockets, Vol 33, pp 734-738, 1996.

Bonfiglio, E. P., Oh, D., and Yen, C-W, **Analysis Of Chemical, REP, And SEP Missions To The Trojan Asteroids**, AAS 05-396, 2005

Botter, T. et al., **Structural Dynamics Of A Spin-Stabilized, Mast-Free Solar Sail Design**, Advances in the Astronautical Sciences. Vol. 124, No. II, pp. 1935-1954, 2006.

Botter, T, Coverstone, V. L. and Burton, R., **Structural Dynamics of Spin-Stabilized Solar Sails with Applications to UltraSail**, Journal of Guidance, Control, and Dynamics, Vol. 31, No. 2, 402-413, 2008.

Brogan, W. L., **Modern Control Theory**, Englewood Cliffs: Prentice Hall, 1991.

Bryson and Ho, **Applied Optimal Control**, Hemisphere Publishing Corporation, 1975.

Burton, R. L., Coverstone, V. L., Hargens-Rysanek, J., Ertmer, K. M., Botter, T., Benavides, G., Woo, B., Carroll, D. L., Gierow, P., Farmer, G., and Cardin, J., **UltraSail, Ultra-Lightweight Solar Sail Concept**, AIAA No. 2005-4117, 2005.

Cal Poly San Luis Obispo, **CubeSat Design Specifications Revision 12**, http://cubesat.org/images/developers/cds_rev12.pdf, 2009.

Cal Poly San Luis Obispo, **CubeSat P-POD Mark II Rendering**, <http://cubesat.org/index.php/media/pictures/55-p-pod-mk-ii-renderings>, 2010.

Chobotov, V., **Orbital Mechanics, 3rd Edition**, AIAA Education Series, 2002

Edelbaum, T. N., **Propulsion Requirements for Controllable Satellites**, ARS Journal, Vol. 31, 1079-1089, 1961.

Edelbaum, T. N., **Optimum Low-Thrust Transfer between Circular and Elliptic Orbits**," Proc. Fourth Nat. Cong. Appl. Mech., (ASME, N. Y.) pp. 137-141, 1962.

Ertmer, K., **Design and Operation of a Thin-Film Vacuum Deployment Experiment for UltraSail Concept Validation**, MS Thesis, Dept. of Aerospace Engineering, University of Illinois, 2006.

Gaposchkin, E.M., **Calculation of Satellite Drag Coefficients**, Technical Report 998, Lincoln Laboratory, MIT, Lexington, Massachusetts, 18 July, 1994.

Goldberg, D. A., **Genetic Algorithms in Search, Optimization, and Machine Learning**, Boston: Addison Wesley Longman, Inc., 1989.

Hargens-Rysanek, J., **The Dynamics and Control of the UltraSail System**, Ph.D. Thesis, Dept. of Aerospace Engineering, University of Illinois, 2006.

Hargens-Rysanek, J., Coverstone, V. and Burton, R., "Orbital Precession Via Cyclic Pitch For The UltraSail System," Paper No. AAS 07-166, AAS/AIAA Space Flight Mechanics Meeting, Sedona, AZ, January, 2007.

Hughes, P.C., **Spacecraft Attitude Dynamics**, John Wiley and Sons, 1986.

MacNeal, R. H., "The Heliogyro, An Interplanetary Flying Machine," NASA Contractor's Report CR 84460, June 1967.

MacNeal, R. H., "Structural Dynamics of the Heliogyro", NASA-CR-1745A, 1971.

McInnes, C. R., **Solar Sailing: Technology, Dynamics, and Mission Applications**, Springer-Praxis Publishing, Chichester, UK, 1999.

NASA Space Vehicle Design Criteria Guidance and Control, **Spacecraft Aerodynamic Torques**, Report: NASA-SP-8058, Jan 1971.

Naval Research Lab NRLMSISE-00, <http://www.nrl.navy.mil/content.php?P=03REVIEW105>, 2003.

Psiaki, M., **Magnetic Torquer Attitude Control via Asymptotic Periodic Linear Quadratic Regulation**, *Journal of Guidance, Control, and Dynamics*, vol. 24, pp. 386-394, March-April 2001.

Pukniel, A., **Attitude Determination and Three-Axis Control System for Nanosatellites with Magnetic Torque Actuation**, M.S. Thesis, Dept. of Aerospace Engineering at the University of Illinois at Urbana-Champaign, 2006.

Pukniel, A., et al., **A Preliminary Study Of The Dynamics And Control Of The CubeSail Spacecraft**, AAS Paper No. 09-417, 2009 Astrodynamics Specialist Conference, Vol. 135, Advances in the Astronautical Sciences, 2009.

Rowe, W.M., **Sail Film Materials and Supporting Structures for a Solar Sail—a Preliminary Design, Vol. IV**, Jet Propulsion Laboratory, Pasadena, California, October, 1978.

Sinclair Interplanetary, **10mNm-sec Reaction Wheel Datasheet**, <http://www.sinclairinterplanetary.com/10mNm-secwheel2009a.pdf>, 2009.

Vulpetti, G., Johnson, L. and Matloff, G. L., **Solar Sails A Novel Approach to Interplanetary Travel**, New York, Copernicus Books, 2008.

Wie, B., **Solar Sail Attitude Control and Dynamics, Part 1**, Journal of Guidance, Control, and Dynamics, Vol. 27, No.4, July-August 2004.

Wright, J.L., **Space Sailing**, Gordon and Breach, New York, 1992.